Master's thesis

NTNU
Norwegian University of Science and Technology
Faculty of Engineering
Department of Energy and Process Engineering

Tarald Wærness

An experimental study of the effects of turbulence on the performance of a wind turbine model with forward and backward swept blades

Master's thesis in Mechanical Engineering
Supervisor: Tania Bracchi
Co-supervisor: R. Jason Hearst
June 2021

NTNU
Norwegian University of Science and Technology

Tarald Wærness

An experimental study of the effects of turbulence on the performance of a wind turbine model with forward and backward swept blades

Master's thesis in Mechanical Engineering
Supervisor: Tania Bracchi
Co-supervisor: R. Jason Hearst
June 2021

Norwegian University of Science and Technology
Faculty of Engineering
Department of Energy and Process Engineering

NTNU
Norwegian University of
Science and Technology

Preface

This Master's thesis was written at the Fluid Mechanics Laboratory at the Department of Energy and Process Engineering (EPT) at the Norwegian University of Science and Technology (NTNU) during the spring semester of 2021. The thesis is presented as a research article in paper-format to be as close as possible to a finished publication. The style guide provided by the Wind Energy Journal was used as a template. The main document is followed by appendices that include additional information that was not incorporated in the research article, but relevant for the Master's thesis. It should be noted that the original problem description, as included here, was changed throughout the semester. This was primarily due to the major refurbishment project that the wind tunnel at NTNU was undergoing while the experiments were performed. In particular, wake measurements were not performed, as this was considered unattainable in a timely manner without a functioning traverse system. Instead, a larger focus was placed on utilizing the newly installed active grid to control the turbulent inflow conditions.

Tarald Warness

Trondheim, June 2021.

Problem description

A number of studies has been done on swept blades for both MW-scale wind turbines and small-scale wind turbines. Nevertheless, the aerodynamics of a rotor with swept blades needs further investigation. In particular, experimental testing in an advanced wind tunnel such as the one at NTNU has not yet been performed. In the present study, a NTNU wind turbine model with straight blades will be used as a baseline model for the swept blade design. The performances and loads of the two rotors will be compared. The preliminary design is based on the engineering tool ASHES, which is a software that performs integrated analysis of HAWTs. The

goals of the project are:

- Build the model(s).
- Measure thrust and power for different TSR.
- Measure the wake for different TSR

The following tasks are to be considered:

- Perform a detailed literature review on horizontal axis wind turbines with swept blades.
- Get familiar with the experimental setup in the wind tunnel and the data acquisition.
- Analyze the results.

Abstract

The aerodynamic performance of a horizontal axis wind turbine model with forward and backward swept blades was investigated experimentally in a wind tunnel. An active grid produced homogeneous, isotropic, freestream turbulence with turbulence intensities of 3%, 19%, and 23%. Three distinct models with rotor diameters of 0.9 m were manufactured from the same material. A baseline model with straight blades was made as a reference to isolate the effect of blade sweep. The two models with swept blades were created by introducing a pre-bending of the straight wind turbine blades in the rotational plane. They were identical except for the blade sweep direction, either forward or backward swept relative to the rotation of the rotors. The results demonstrate that the straight blades outperformed both the forward and backward swept blades at low turbulence intensities. However, at higher turbulence intensities, the forward swept blades had a 6.0% higher maximum power coefficient at the expense of an increase in the thrust coefficient of 7.1%. The backward swept blades experienced a 4.6% lower maximum power coefficient and a further decrease in the thrust coefficient of 7.6% compared to the straight blades. The relative differences in performance could be associated with how the various models were affected by the freestream turbulence. The swept blades experienced the most significant increase in the power output at higher turbulence intensities, up to 41% for the forward swept blades and 28% for the backward swept blades. These results provide increased motivation to investigate further the effects of turbulence on swept blades.

Sammendrag

Den aerodynamiske ytelsen til en vindturbinmodell med fremover- og bakoverbøyde blader ble undersøkt eksperimentelt i en vindtunnel. Et aktivt turbulensgitter produserte homogen og isotrop turbulens med turbulensintensiteter på 3%, 19% og 23%. Tre forskjellige modeller med rotordiameter på $0,9$ m ble produsert i samme materiale. En modell med rette blader ble laget som en referanse for å isolere effekten av de bøyde bladene. De to modellene med bøyde blader ble produsert ved å introdusere en forhåndsbøyning av de rette vindturbinbladene i rotasjonsplanet. De var identiske bortsett fra den bøyde retningen, enten fremover eller bakover i forhold til rotorenes rotasjon. Resultatene viser at de rette bladene hadde bedre aerodynamisk ytelse enn både de fremover- og bakoverbøyde bladene ved lave turbulensintensiteter. Imidlertid, ved høyere turbulensintensiteter, hadde de fremoverbøyde bladene en $6,0$% høyere maksimal effektkoeffisient på bekostning av en økning i skyvekoeffisienten på $7,1$%. De bakoverbøyde bladene opplevde en $4,6$% lavere maksimal effektkoeffisient og en ytterligere reduksjon i skyvekoeffisienten på $7,6$% sammenlignet med de rette bladene. De relative forskjellene i ytelse kan være assosiert med hvordan de forskjellige modellene ble påvirket av freestream-turbulensen. De bøyde bladene opplevde den største økningen i effekt ved høyere turbulensintensiteter, opp til 41% for de fremoverbøyde bladene og 28% for de bakoverbøyde bladene. Disse resultatene gir økt motivasjon for å undersøke nærmere virkningene av turbulens på bøyde vindturbinblader.

RESEARCH ARTICLE

An experimental study of the effects of turbulence on the performance of a wind turbine model with forward and backward swept blades

Tarald W. Wærness

Energy and Process Engineering, Norwegian University of Science and Technology, Trondheim, Norway

Correspondence
Tarald W. Wærness,
Email: tarald.waerness@gmail.com

Abstract

The aerodynamic performance of a horizontal axis wind turbine model with forward and backward swept blades was investigated experimentally in a wind tunnel. An active grid produced homogeneous, isotropic, freestream turbulence with turbulence intensities of 3%, 19%, and 23%. Three distinct models with rotor diameters of 0.9 m were manufactured from the same material. A baseline model with straight blades was made as a reference to isolate the effect of blade sweep. The two models with swept blades were created by introducing a pre-bending of the straight wind turbine blades in the rotational plane. They were identical except for the blade sweep direction, either forward or backward swept relative to the rotation of the rotors. The results demonstrate that the straight blades outperformed both the forward and backward swept blades at low turbulence intensities. However, at higher turbulence intensities, the forward swept blades had a 6.0% higher maximum power coefficient at the expense of an increase in the thrust coefficient of 7.1%. The backward swept blades experienced a 4.6% lower maximum power coefficient and a further decrease in the thrust coefficient of 7.6% compared to the straight blades. The relative differences in performance could be associated with how the various models were affected by the freestream turbulence. The swept blades experienced the most significant increase in the power output at higher turbulence intensities, up to 41% for the forward swept blades and 28% for the backward swept blades. These results provide increased motivation to investigate further the effects of turbulence on swept blades.

KEYWORDS:
swept blades, wind tunnel experiments, wind turbine performance, freestream turbulence

1 | INTRODUCTION

Wind energy is predicted to be one of the main contributors to the growth in renewable energy production over the next decades [1]. Continuously researching and finding new, more efficient technologies are of utmost importance if the world is to transition to a more sustainable future with clean, renewable electricity production. Today, the most widely used wind turbine design is horizontal axis wind turbines with three blades [2]. Over the last few decades, there has been a significant increase in the total power output of these wind turbines, mainly because of larger rotor diameters [3]. Still, to ensure continued growth, increasing the aerodynamic efficiency of wind turbines through innovations in the rotor blade design is also necessary [4]. In addition, due to the larger rotor diameters of the wind turbines, the experienced loads have increased, which results in higher maintenance costs and lower life expectancy [5]. Therefore, increasing the aerodynamic efficiency and reducing the loads on the wind turbine blades could help lower the cost of energy and increase the life expectancy of wind turbines, making wind energy a more viable alternative to fossil

fuels. Horizontal axis wind turbine blades can be found in many different shapes and forms [6]. A recent development, made possible by advances in manufacturing, introduces a curve in the shape of the blades [7]. In particular, swept blades are produced by pre-bending the wind turbine blades in the rotational plane. This is a newly developed concept that has shown promising results to yield increased energy capture without increasing the turbine loads [8,9].

Several studies have been performed on horizontal axis wind turbines with swept blades. The most complete study on the subject is the development of the Sweep-Twist Adaptive Rotor (STAR) that was conducted by the Knight & Carver Wind Group [10,11,12]. The study consists of aeroelastic simulations, manufacturing, and testing, and was based on the early works of Zuteck et al. [8] and Ashwill et al. [9].

Most recent studies on swept blades utilize the well-established Blade Element Momentum (BEM) method, with varying degrees of complexities [13,14,15,16,17]. Hansen [18] investigated the static and dynamic aeroelastic properties of backward swept blades. A detailed parametric study involving geometric parameters for swept blades was conducted by Verelst & Larsen [19]. Larwood et al. [20] performed a design study of swept wind turbine blades that showed a 5% increase in the annual energy production over the straight blade model. The study showed that the most sensitive parameter to load reduction was the amount of tip sweep. In addition, Larwood et al. [21] also developed an improved aeroelastic code to analyze the swept blades.

A new wind tunnel study, performed by Barlas et al. [22], investigated a swept tip shape both experimentally and numerically. The wind tunnel tests consisted of performing measurements on a single, swept blade at different angles of attack and wind speeds. Although wind tunnel measurements were performed to assess wind turbines with swept blades, Barlas et al. [22] did not produce a fully functional wind turbine model. Their experiments were mostly intended as reference for different numerical approaches.

Other studies include Computational Fluid Dynamics (CFD) analyses, which could potentially give some indication of the overall performance characteristics of a wind turbine with swept blades [23]. Khalafallah et al. [24] analyzed a broad range of design parameters and directions of the curvature of the blades. In particular, they included an analysis of upstream and downstream curved blades, in addition to forward and backward sweep. They used a baseline model to compare the aerodynamic performance of the CFD results for the modified wind turbines and several different equations for the sweep curves. They concluded that the downstream curved blades showed the most significant increase in the power output of up to 3.47%, but they also found a slight increase for the forward swept blades. Kaya et al. [25] explored the aerodynamic performance of a horizontal axis wind turbine with forward and backward swept blades. They used the same baseline model as Khalafallah et al. [24], a small horizontal axis wind turbine with straight blades developed at the Norwegian University of Science and Technology (NTNU). In particular, they analyzed the power coefficients of the wind turbines, which is given by

$$C_P = \frac{P}{\frac{1}{2}\rho U_\infty^3 A}, \tag{1}$$

where ρ is the air density, U_∞ is the velocity of the incoming wind, and $A = \pi R^2$ is the total sweep area of the rotor [18]. They found an increase in the power output of 2.9% over the baseline turbine for the forward swept blades at the design tip speed ratio. The tip speed ratio of a wind turbine is given by

$$\lambda = \frac{\omega R}{U_\infty}, \tag{2}$$

where ω is the angular velocity of the rotor and R is the radius of the blades. In the same study, they found a decrease in the thrust coefficient of 5.4% for the backward swept blades. The thrust coefficient of a wind turbine is defined as

$$C_T = \frac{F_T}{\frac{1}{2}\rho U_\infty^2 A}, \tag{3}$$

where F_T is the total thrust force acting on the rotor. Their CFD study concluded that forward swept blades could increase the power output of a wind turbine, while backward swept blades could potentially decrease the thrust coefficient, and therefore the loads acting on the wind turbine.

Previous studies have investigated the effects of freestream turbulence (FST) on the power output and loads of horizontal axis wind turbine models [26,27,28]. However, the advent of active grids, as introduced by Makita [29], has expanded the range of possibilities within this field. The active grids allow for augmenting the turbulence produced downstream in a controlled sequence. In particular, random motions can produce freestream turbulence that is approximately homogeneous and locally isotropic [30,31]. In addition, active grids have allowed for obtaining much higher turbulence intensities than previously. This is beneficial in wind turbine studies in particular since the atmospheric boundary layer (ABL) that utility scale wind turbines operate in typically have turbulence intensities between 5% and 15%, with gusts reaching up to more than 40% [32]. The turbulence intensity is defined as

$$T_i = \frac{\langle u'^2 \rangle^{1/2}}{U_\infty}, \tag{4}$$

where u' is the time-varying stream-wise velocity fluctuations, U_∞ is the mean stream-wise velocity, and $\langle\cdot\rangle$ denotes the time average. Gambuzza et al.[33] performed wind tunnel measurements on a small model wind turbine using an active grid. They showed that the power output was highly affected by the inflow turbulence characteristics, with an increase of up to 16% between the maximum power coefficients for the low and high turbulence test cases. The thrust was relatively constant throughout the measurements. Their active grid produced a variety of inflow conditions, with varying turbulence intensities and integral length scales. The integral length scale, L_{ux}, is a measure of the largest turbulence structure in the flow. Li et al.[34] performed measurements on a small wind turbine model with an active grid, and placed specific focus on decoupling the shear from the turbulence intensity. Rockel et al.[35] used an active grid in passive and active modes to create inflow conditions with low and high turbulence. Talavera & Shu[36] created three different simulations of turbulent atmospheric boundary layers (ABLs) using a single active grid setup, with turbulence intensities ranging from 3% to 17% at the centre of the turbine. Jin et al.[37] explored the flow structure in the wake of a model wind turbine under negligible and high turbulence in the freestream region of a wind tunnel. Attention was placed on the evolution of the integral length scale and the contribution of the large-scale motions from the background flow.

The present study aims to further investigate the differences found in other studies on the aerodynamic performance of swept blades. This study performs wind tunnel measurements, whereas most other studies on swept wind turbine blades have been numerical. Since the standard BEM methods are two-dimensional and the computational time and resources needed for CFD analyses are high, it is generally challenging to assess complex systems such as horizontal axis wind turbines (HAWTs)[38]. This is particularly true for HAWTs with swept blades, and therefore, performing wind tunnel experiments could be a more feasible alternative to produce accurate results. In addition, wind tunnel studies on wind turbine models with swept blades is a topic that is not very well covered. In particular, the impact of freestream turbulence (FST) is seemingly absent from the literature. Thus, this study focuses on the effect of varying the turbulent inflow conditions with an active grid, while the reference velocity is kept constant at $U_\infty = 12.5$ m/s. The active grid was operated in fully random modes, to produce homogeneous freestream turbulence, with different turbulence intensities and integral length scales. To isolate this effect on the performance of a wind turbine model with forward and backward swept blades, three distinct models were designed and produced by the author. A wind turbine model with straight blades was used as reference, and the two wind turbine models with swept blades were identical except for the blade sweep direction, either forward or backward with regards to the rotational direction.

2 | METHODOLOGY

2.1 | Wind tunnel

The experiments were performed in a large-scale, closed-return wind tunnel in the Fluid Mechanics Laboratory at the Norwegian University of Science and Technology (NTNU). The wind tunnel has a test section of 1.80 m (height) x 2.71 m (width) x 11 m (length). The wind tunnel has been used in numerous wind turbine studies[39,40,41,42]. However, as it is newly refurbished, this study is the first of its kind in the current configuration of the wind tunnel. The wind tunnel operates at a broad range of freestream velocities, between 0 and 25 m/s. For this study, as mentioned, the reference velocity was kept at a constant $U_\infty = 12.5$ m/s for all the test cases. The choice of reference velocity was a trade-off between increasing the Reynolds number in the wind tunnel tests and the physical and safety limitations regarding the newly installed wind tunnel walls, the active grid operating range, and the wind turbine models themselves. This is discussed in more detail in Section 3.1.

2.2 | Active grid

An active grid was used to generate highly turbulent inflow conditions; see Figure 1. The active grid has the same cross-section as the wind tunnel (1.80 m x 2.71 m) and is currently one of the physically largest active grids in the world[43]. The active grid is made of orthogonal rods with vanes attached to them. Each vertical rod includes 18 diamond vanes with a diagonal of 95 mm (69 mm x 69 mm). The horizontal rods include 27 similar vanes. The vanes are evenly spaced, resulting in a mesh length of M = 100 mm. Due to the large size of the grid, the interior support structure is present. A horizontal bar is located at mid-height, giving a blockage of 9.7 mm, which is similar to the blockage from the rods. In addition, three 12.7 mm thick vertical bars are located at the center of the structure, as well as 700 mm on either side of the center. In total, the active grid consists of 90 shafts (rods with vanes), where each shaft is controlled by a dedicated integrated stepper motor (Applied Motion Products Model No. STM23S-3RE). Each motor includes an integrated drive and encoder.

To achieve homogeneous, isotropic turbulence, the shafts were operated in fully random modes, with randomized acceleration, periods of rotation, and rotation frequency. The shafts were controlled individually using a MATLAB script, where the implemented driving algorithm created a fully random sequence, as proposed by Hearst & Lavoie[31]. This allowed for varying the rotation frequency, $\Omega \pm \omega'$, of the rods in the active grid to produce the turbulent test cases presented in Table 1. Due to the arbitrary nature of the rotations, ω' is a random frequency up to $\frac{1}{2}\Omega$.

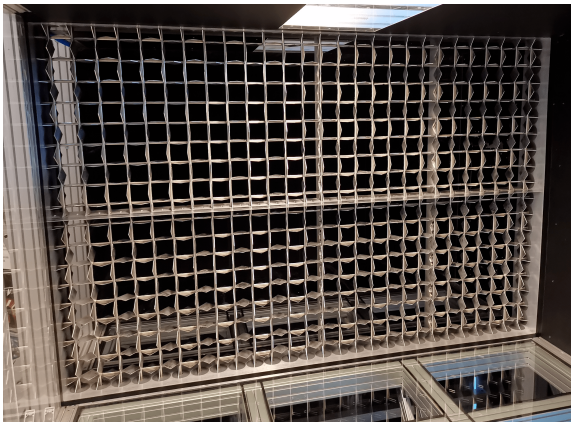

FIGURE 1 The active grid that was used in this study, seen from downstream and depicted in static mode (test case L03).

Hot-wire measurements were performed using a Dantec 55P21 X-wire probe controlled via a Dantec StreamLine Pro Constant Temperature Anemometer. The wires have a diameter of 5 μm and a sensing length of 1.25 mm. The tip of the X-wire probe coincided with the hub location. The characterizations were performed with the same wind tunnel speed setting for each case. The data acquisition was conducted through a computer with a NI DAQ system. The X-wires were operated at an overheat ratio of 1.8, and data were sampled at 5 kHz, with the internal anemometer low-pass filter set at 30 kHz. The sampling time varied from 300 s to 600 s depending on the active grid cases. The spectra of the raw X-wire signals were checked after each acquisition to ensure convergence in the low-frequency content.

In order to analyze the effects of freestream turbulence (FST) on the wind turbine performance, a reduced set of parameters were used, namely the turbulence intensity, T_i, and the integral length scale, L_{ux}. The integral length scale is usually normalized by a relevant dimension, and therefore L_{ux}/D is used in this study, where $D = 2R$ is the turbine diameter. Table 1 shows an overview of the measured turbulence characteristics, in terms of the turbulence intensities and integral length scales of each of the test cases in this study. The turbulence characteristics are coupled, meaning both the turbulence intensity and integral length scale increase simultaneously, and are inversely proportional to the mean rotation frequency of the grid [31], Ω. In addition, a case without the active grid was analyzed. A section with solid walls on all sides replaced the active grid to provide a clean inlet flow in the wind tunnel after it was removed.

To differentiate between the test cases a naming convention was developed for the incoming flow fields. The baseline case with no grid is denoted as REF for reference. The FST test cases with the active grid are described with a letter, L, M, or H, for low, medium, and high values of the integral length scales (L_{ux}/D). In addition, numbers for the measured turbulence intensities are added for the active grid test cases. An overview of the full range of FST test cases that could be generated with the fully random modes can be seen in Table A1 in Appendix A. Unfortunately, it was not was not possible to produce turbulence intensities between 3% and 18% for the current configuration. While the author recognizes that this imposed a limitation, the main purpose of this study was to analyze the effects of blade sweep at the same turbulent inflow conditions. Thus, the selected FST test cases were considered sufficient.

TABLE 1 Overview of the inflow conditions for each test case.

Test Case	Active grid	$\Omega \pm \omega'$ [Hz]	T_i [%]	L_{ux}/D	U_∞ [m/s]
REF	No		1.0		12.5
L03	Yes	0.0 ± 0.0	2.87	0.049	12.5
M19	Yes	5.0 ± 2.5	18.82	0.281	12.5
H23	Yes	1.0 ± 0.5	22.60	0.483	12.5

Note: The integral length scale, L_{ux}, and rotation frequency, Ω, of the active grid are not applicable for the clean inlet flow (REF).

2.3 | Wind turbine models

In total, three wind turbine models were produced for this study. A model with straight blades was made as a reference, in addition to the two distinct models with swept blades. The difference in the design of the resulting wind turbine models was the blade sweep orientation, either forward or backward swept, with respect to the rotational direction of the rotor. All three wind turbine models were produced in the same material

to eliminate the potential influence of disparate material properties. Ebaboard PW920 was chosen because of its relatively high stiffness and edge stability. In addition, it is a less costly and more workable material compared to other stiffer materials such as aluminum. A CNC machine at the Fluid Mechanics Laboratory was used to cut out the wind turbine blades from one solid piece of the material. After being cut, the blades were sanded with varying grades of sandpaper to remove additional support structures. The finest grade was P1000, resulting in a smooth finish throughout the blade span. The wind turbine blades in this study were adopted from a baseline wind turbine model with straight blades that has previously been tested extensively in the wind tunnel at NTNU [44,45,46]. The geometry of the blades was developed using a Blade Element Momentum method with Prandtl's tip loss model and Glauert's correction for the thrust force incorporated [44]. The design tip speed ratio was set to $\lambda = 6$. The baseline model consists of straight blades with the NREL S826 airfoil throughout the blade span [45]. This profile was specifically designed for wind turbines and was considered well suited for wind tunnel experiments. In particular, it has a separation ramp at the back that was designed to give high maximum lift, gentle stall, and insensitivity to surface roughness [47]. The NREL S826 profile appears in Figure 2. A previous study conducted by Li et al. [48] investigated the influence of freestream turbulence on the lift of the NREL S826 airfoil. It was found that an increase in T_i increases the maximum lift for this particular airfoil, especially at higher turbulence intensities. For some of the lower turbulence intensities, the lift decreased slightly.

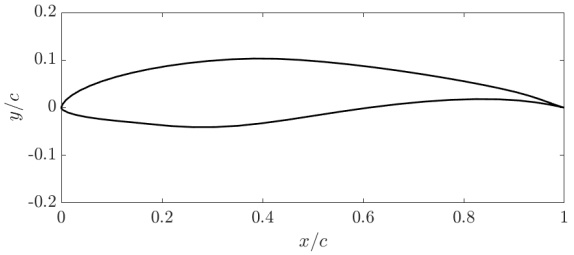

FIGURE 2 The NREL S826 airfoil that was implemented in the wind turbine models.

The blade characteristics, given by the blade twist angle, ϕ, and normalized airfoil chord length, c/R, for each blade element with normalized local radius, r/R, are shown in Figure 3. Towards the root of the blade ($r/R < 0.1$) the NREL S826 airfoil was replaced by a cylinder with $d = 0.025$ m to be more easily attached to the hub (see Figure 4). For this wind turbine model, the chord length is about three times wider than what is typical for commercial wind turbines. The primary purpose of the relatively wide blades was to help reduce the gap in Reynolds numbers. This is beneficial in wind tunnel experiments where Re is inevitably much lower than for utility-scale wind turbines [45].

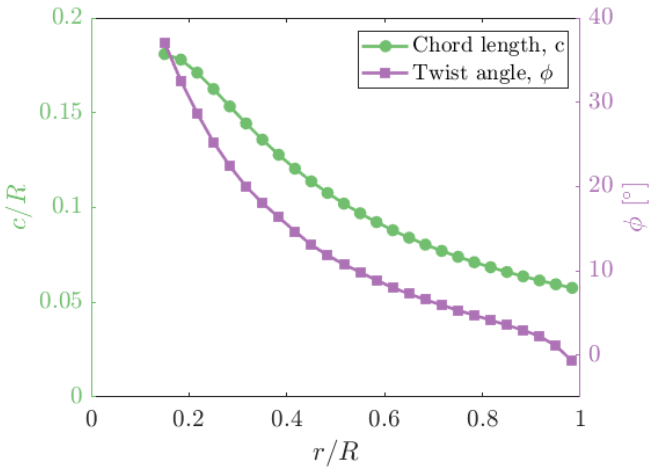

FIGURE 3 Chord length and twist angle distribution for each blade element, adopted from Krogstad et al. [44]. The values were used for all the wind turbine models in this study.

Among the many approaches for designing the curve of a swept blade, Kaya et al. [25] created an equation to easily specify the design parameters for blade sweep startup, $P_{rss} = r_{ss}/R$, and tip offset, $P_{ds} = d_s/R$, relative to the blade radius. This equation is given by

$$Z_s = \frac{(r_r - r_{ss})P_{ds}R/(R - r_{ss})}{M_s^{((1-P_r)(1-P_{rss})/P_r)}}, \tag{5}$$

TABLE 2 Overview of the wind turbine models that were used in this study.

Test Case	Blade Sweep	Material	R [m]	$\mathbf{P_{rss} = r_{ss}/R}$	$\mathbf{P_{ds} = d_s/R}$
F	Forward swept	Ebaboard PW920	0.45	0.35	0.20
B	Backward swept	Ebaboard PW920	0.45	0.35	0.20
S	Straight	Ebaboard PW920	0.45	0.00	0.00

where Z_s is the sweep offset in the rotational plane, r_r is the projected radial distance of each element onto the pitch axis, r_{ss} indicates the sweep startup, and M_s is a constant that dictates the strength of the sweep. The approach of Kaya et al.[25] was chosen for this study, for comparison purposes. In a preliminary study, the author developed and analyzed a total of 12 blade designs based on the two design parameters, P_{rss} and P_{ds}. The maximum values for the parameters were set to $P_{rss} = 0.55$ and $P_{ds} = 0.20$, respectively. Also, the sweeping strength was set to $M_s = 4$ as this gave a more realistic curve that was thought to be easier to replicate in an actual blade. This differs slightly from the method used by Kaya et al.[25] as they used $M_s = 2$. The preliminary study used the well-established Blade Element Momentum (BEM) method, with 30 elements throughout the blade span (as in Figure 3). The software ASHES[49] incorporates a standard implementation of the BEM method with a recently added ability of analyzing swept blades. The results from ASHES showed that the most interesting effects were found with the highest degree of blade sweep (maximum value of tip offset, $P_{ds} = 0.20$). This was in line with the CFD results of Kaya et al.[25] and supported by several other studies[20]. However, for the blade sweep startup, the results differed. Here, the CFD study of Kaya et al.[25] found that an earlier sweep startup would increase the power output ($P_{rss} = 0.15$), while the ASHES study conducted by the author indicated that a late sweep startup could be beneficial ($P_{rss} = 0.55$). The main results from this preliminary study are presented in Appendix B.

As a result of this, and considering the physical limitations of the manufacturing process, it was decided to use the following design parameters for both the forward and backward swept blades in this study: $P_{ds} = 0.20$ and $P_{rss} = 0.35$. Table 2 summarizes the most important information about the resulting wind turbine models with swept blades. In addition, to isolate the effect of blade sweep on the wind turbine blades, a separate wind turbine model with straight blades was produced. Thus, a total of nine wind turbine blades, three blades for each of the three distinct wind turbine models, were produced in this study. These are shown in Figure 4.

Generally, the performance of a wind turbine is affected by changes in the rotor-swept area and the rotor solidity[50]. The radius was kept constant for all the blades to eliminate the influence of the rotor-swept area, $A = \pi R^2$. The swept blades experience a slight increase in the rotor solidity, defined as the total blade area divided by the rotor-swept area. The curved length of the swept blades covers a slightly more significant part of the rotor-swept area than the straight blades. However, since the forward and backward swept blades were identical except for the sweep direction, their solidity was equal.

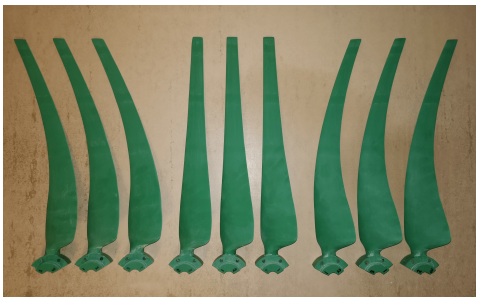

FIGURE 4 The wind turbine blades that were produced in this study, in Ebaboard PW920 (back view). Forward swept (left), straight (middle), backward swept (right). Each set of three blades were mounted to the experimental setup with two metal clamps.

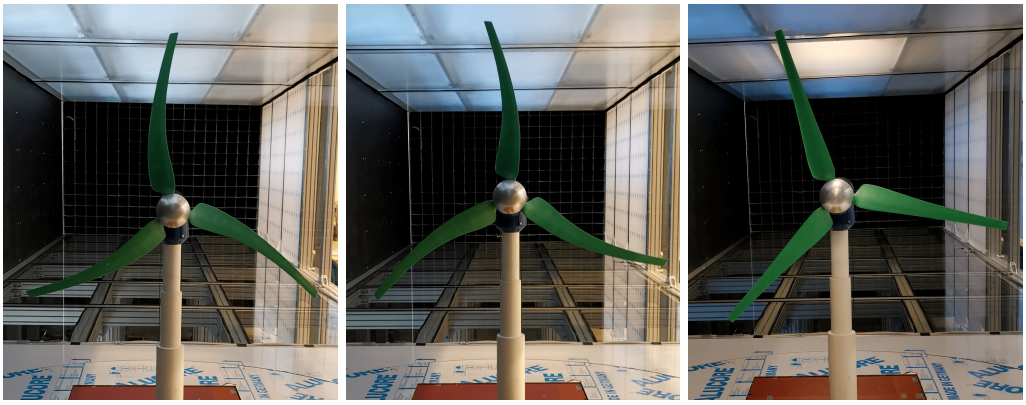

FIGURE 5 Front view of the wind turbine models attached to the experimental setup, with an aluminum hub that attached to the blades. **(a)** forward swept blades (F), **(b)** backward swept blades (B), **(c)** straight blades (S). The rotational direction was clockwise for all the models.

2.4 | Experimental setup

The wind turbine models were attached to an experimental setup used in several previous studies[44,45], and is shown in Figure 5. It consists of a tower shaft and nacelle, with a rotor shaft inside the nacelle that connects directly to an electric motor with a belt drive. The rotor shaft has a metal plate at one end, so that the wind turbine models could be mounted directly to it. An aluminum hub with a diameter of 90 mm used in previous studies[44] was redesigned to fit with the current setup. It attached directly to the wind turbine models and could be used for all three models to ensure that the only difference between the models were the wind turbine blades themselves. Figure 6 shows a 2D overview of the experimental setup in the wind tunnel. Figure 7 shows a picture of one of the wind turbine models and the active grid during operation. The hub height was $H = 820$ mm above the wind tunnel floor. The distance from the wind tunnel inlet to the installed active grid was 0.7 m and the width of the support structure of the grid was 0.3 m. The latter is the section that was removed and replaced by solid walls to provide a clean inlet flow for the REF test case in Table 1. The distance from the active grid to the hub's location was 3 m, resulting in a relative streamwise distance of $x/M = 30$, where $M = 100$ mm is the mesh length of the grid. In previous studies, this has been found to be far enough downstream to consider the freestream turbulence homogeneous and isotropic for the active grid modes presented in Section 2.2[31,30]. In addition, homogeneity scans were performed slightly further downstream from the hub location, adding to the validity of this assumption[51].

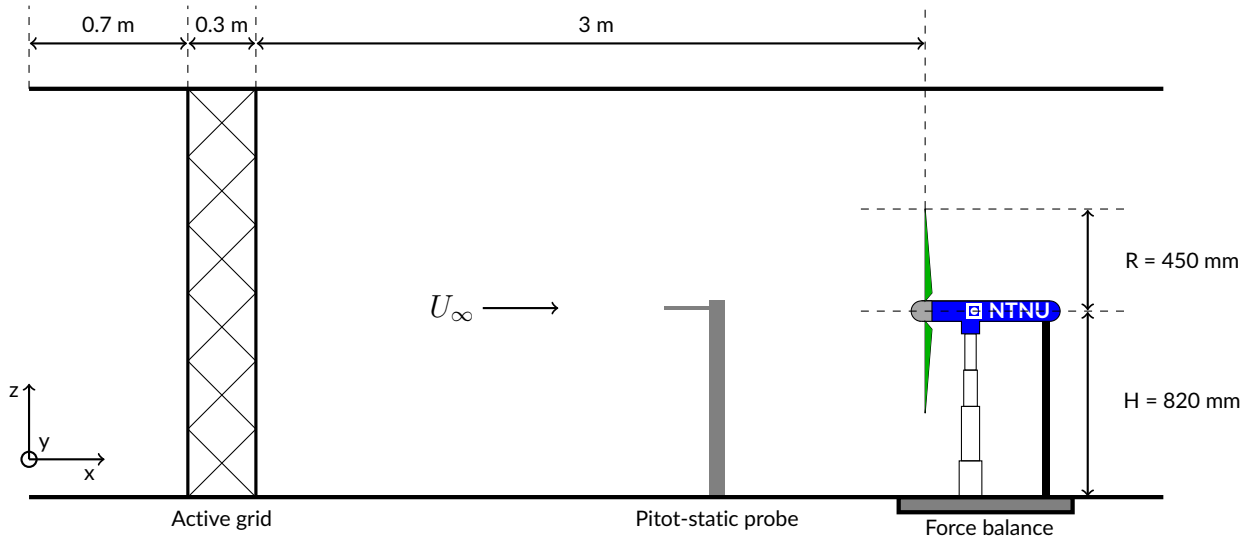

FIGURE 6 Schematic of the side view of the experimental setup in the wind tunnel. The Pitot-static pressure probe was mounted slightly to the right (y-direction) of the wind turbine model so that it would not interfere with the turbine measurements. The drawing is to scale.

The lowest elevation of the blade during rotation was 370 mm, which has been measured in previous studies to be outside of the ground plane boundary layer in the wind tunnel[45]. The rotor speed of the wind turbine models was controlled and monitored by a SIEMENS MICROMASTER 440 frequency converter connected to a 0.43 kW SIEMENS AC electric motor, with a maximum rotational speed of about 3000 rpm. This allowed for varying the rotational velocity of the wind turbine models in the range of $20 \lesssim \omega \lesssim 300$ [rad/s]. The corresponding tip speed ratio range was $1 \lesssim \lambda \lesssim 10$, which was more than sufficient for the wind turbine models studied herein. The excess power produced during the experiments was dissipated in a variable resistor connected directly to the frequency converter with electric test leads.

The model blockage ratio, which is the ratio between the rotor-swept area, A, and the wind tunnel cross-sectional area, A_t, was 13% in this study. Even though the blockage ratio was similar in previous studies[44,45], it should be noted that it is slightly higher than recommended and close to the limit where the potential blockage effects could have a significant influence on the results[52]. However, the main purpose of this study was to compare the aerodynamic performance of the various blade designs. Thus, it was deemed appropriate to test the wind turbine models with a relatively high blockage ratio for the added benefits of utilizing a well-functioning experimental setup with many readily available reference studies already performed on similar wind turbine models.

2.5 | Measurement equipment and uncertainties

A torque transducer measured the aerodynamic power of the wind turbine models, $P = Q\omega$, where Q is the net torque measured by the transducer. The bottom of the tower shaft was mounted to a six-component force balance to measure the thrust forces acting on the models. Both instruments were calibrated before testing using standard weights. The torque transducer also had an electronic speed of rotation output used to calculate the angular velocity of the rotor, ω. The output data were acquired using in-house LabVIEW software, at a sampling rate of 2000 Hz and for a total of 30 seconds for each sample. The freestream reference velocity was measured using a Pitot-static pressure probe mounted upstream and slightly to the side of the wind turbine. A wall-mounted thermometer measured the temperature in the wind tunnel, and a precision mercury manometer measured the atmospheric pressure in the facility. Beforehand, to ensure consistency, a match with previous results obtained with the same measurement equipment was checked, see Appendix A.

The total measurement uncertainties were obtained for every measurement point by a combination of random and systematic uncertainties as proposed by Wheeler et al.[53]. The random uncertainties were computed for a 95% confidence interval from the measured signals. Due to the high number of measurements, the random uncertainty was relatively small, even for the highly turbulent test cases where the variance in the measurements was more significant than in the low turbulence test cases. The systematic uncertainties in the measurement equipment were found to be the major contributors to the overall uncertainties. In particular, the systematic error of the Pitot-static pressure probe and the corresponding error in the mean reference velocity was found to be the largest at about $\pm 1\%$. Thus, the calculated power coefficients, C_P, presented in this study, were found to be within $\pm 3\%$ of the mean values. The calculated thrust coefficients, C_T, had a slightly lower uncertainty of around $\pm 2\%$ throughout the experiments. The procedure for calculating the uncertainties are detailed in Appendix C.

FIGURE 7 A wind turbine model and the active grid, depicted while rotating.

3 | RESULTS AND DISCUSSION

The overall behavior of the power output and thrust at different wind speeds dictates the aerodynamic performance of a wind turbine model. While operating at a constant wind speed, the power coefficient, C_P (1), and the thrust coefficient, C_T (3), at a wide range of tip speed ratios, λ (2) can be calculated by varying the rotational velocity of the rotor. The following section presents mean values and the corresponding uncertainties of the power and thrust coefficients for the wind turbine models detailed in Table 2 and inflow conditions described in Table 1. To increase the readability the error bars only highlight the most interesting tip speed ratio range, but the errors were relatively constant for all the measurements, as explained in Section 2.5. First, the Reynolds number dependence in this study is discussed. In particular, the results from the REF test case showed a behavior for the power coefficient that is typically present when the Reynolds number is too low. This was not found for the low turbulence test case, L03, where the power curves for all the wind turbine models exhibited the expected characteristics. The results from the medium and high turbulence test cases (M19 and H23) were very similar, and M19 was therefore considered representative. Thus, more emphasis was placed on the results from the low turbulence test case L03 and the medium turbulence test case M19, of which the main analysis in this section was performed, for all three wind turbine models denoted by F, B, and S. The results from test cases REF and H23 are shown in Appendix D, in addition to supplementary figures from test cases L03 and M19 that were not included in the main results.

3.1 | Reynolds number dependence

For a horizontal axis wind turbine, the Reynolds number at the blade tip, denoted as the tip Re, is given by $Re = \frac{\omega R c}{\nu}$, where c is the chord length at the blade tip and ν is the kinematic viscosity. The performance of a model wind turbine is generally highly dependent on Re, and thetherefore the freestream velocity, U_∞. However, at a certain threshold, the power and thrust coefficients tend to become independent of the freestream velocity. This is important in wind tunnel studies in particular where Re is inevitably lower because of the much smaller model scale compared with utility-scale wind turbines. In previous studies on the baseline model with aluminum blades[44,45], it was found that Re independent behaviour occurred at $U_\infty > 9$ m/s. Therefore, most studies have been performed at a reference velocity of $U_\infty = 10$ m/s, as this was found to be sufficiently high.

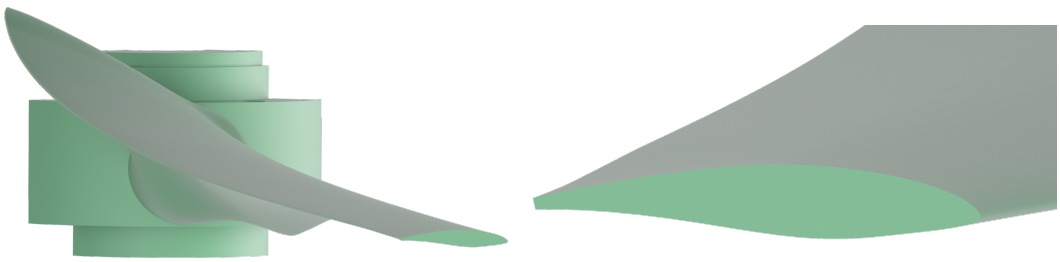

FIGURE 8 Side views of the CAD model for the straight wind turbine blades produced in this study. Full blade view of the tolerance of 0.6 mm at the trailing edge (left). Zoomed in view of the blade tip, showing the resulting airfoil profile (right).

In this study, the tolerance at the trailing edges of the airfoils was 0.6 mm throughout the blade span due to the chosen manufacturing process. Figure 8 illustrates how the resulting airfoil profiles were affected by the relatively high tolerance. Notice how the tip of the blades was particularly affected, where the trailing edge is cut off, compared to the NREL S826 profile shown in Figure 2. This effect was less prevalent in previous studies where aluminum blades were used, as the tolerance, in that case, was much lower. Reducing the airfoil chord length, c, directly decreases the experienced Reynolds number. A detailed study on the Reynolds number dependency was not performed for these blades. However, preliminary results conducted by the author showed that the power and thrust coefficients were still Re dependent at $U_\infty = 10$ m/s for the Ebaboard PW920 blades studied herein. Consequently, the freestream velocity was increased to $U_\infty = 12.5$ m/s throughout the experiments. Even at this higher reference velocity, some of the results exhibited an unexpected behavior for the power and thrust coefficients around the design tip speed ratios. This was particularly noticeable for the forward and backward swept blades without the active grid (test case REF), where the power output was much lower than expected at $\lambda = 6$ (see Figure D7a in Appendix D). The reduced chord length discussed above might explain some of this behavior. Increasing the reference velocity above $U_\infty = 12.5$ m/s could be helpful to counteract this effect. However, limitations on the operating range of the active grid and safety concerns with the wind turbine models made it difficult to obtain results at higher velocities in this study. Previous studies have shown that the Reynolds number effect is also dependent on the freestream turbulence[54]. This was found to be the case for this

study as well, where a small increase in the turbulence intensity resulted in much less Re-dependent behavior, as depicted in Figure 9a. Therefore, the reference velocity of $U_\infty = 12.5$ m/s was considered satisfactory.

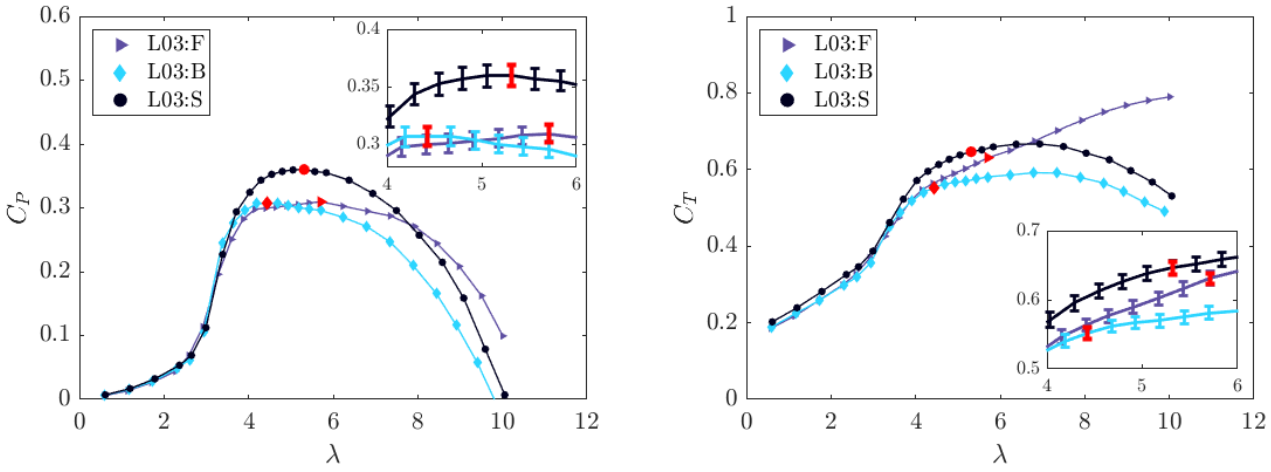

(a) (b)

FIGURE 9 Effects of blade sweep for the wind turbine models with forward swept (F), backward swept (B) and straight (S) blades. **(a)** power coefficients and **(b)** thrust coefficients at different tip speed ratios, λ. The figure depicts the low turbulence test case, L03, with $T_i = 2.87\%$ and $L_{ux}/D = 0.049$. The reference velocity was kept constant at $U_\infty = 12.5$ m/s for all the test cases. Thus, the tip speed ratio was only varying with the rotational velocity of the rotors, ω. The data points highlighted in red indicate the locations of the maximum power coefficients, $C_{P_{max}}$, for each test case. Error bars for C_P and C_T are shown in a zoomed view for the most interesting parts of the data.

3.2 | Effects of blade sweep

The main part of this study was to analyze the differences in the aerodynamic performance of a wind turbine model with forward and backward swept blades. Figure 9 shows the calculated performance characteristics for the forward swept blades (F), backward swept blades (B), and straight blades (S) at low FST ($T_i = 2.87\%$ and $L_{ux}/D = 0.049$). For the low turbulence test case L03, where the installed active grid was in static mode, the straight blades outperform the swept blades, regardless of the sweep direction. The only exceptions were at high tip speed ratios, $\lambda > 8$, where the forward swept blades (B) have the highest power output. The power coefficients for all the models follow a wind turbine's expected power curve characteristics (see Figure 9a). The power coefficients increase with the tip speed ratio, attain a maximum value, and decrease with a further increase in the tip speed ratio. The main difference caused by the blade sweep direction at low turbulence was a reduction in the experienced thrust force for the backward swept blades (B). The maximum values for the power coefficients, $C_{P_{max}}$, were 14.1% and 14.7% lower for the forward and backward swept blades, respectively, compared to the straight blades. The corresponding decrease in thrust coefficients at the same tip speed ratios was 2.4% for the forward swept blades (F), and 14.6% for the backward swept blades (B). Thus, it becomes clear that the backward swept blades experience a more significant decrease in the thrust coefficient at approximately the same maximum power output as the forward swept blades. Table 3 summarizes these findings for both the low and medium turbulence test cases, where the extracted data points for the maximum power coefficients, $C_{P_{max}}$, highlighted in red in Figure 9 are shown with their corresponding uncertainties. An additional evident effect from Figure 9a is that the forward swept blades seem to retain a relatively high power output close to the $C_{P_{max}}$ for a much broader tip speed ratio range. On the contrary, the power output of backward swept blades drop off quite substantially at tip speed ratios greater than the design value ($\lambda > 6$). Figure 9b shows how this behavior manifests in the thrust coefficients at higher tip speed ratios, where the experienced loads were almost twice as high for the forward swept blades (F) as for the backward swept blades (B) at $\lambda \approx 10$. At low tip speed ratios, $\lambda < 4$, the backward swept blades (B) seem to experience a slightly higher power output than the forward swept blades (F). This is discussed in more detail in Appendix D.

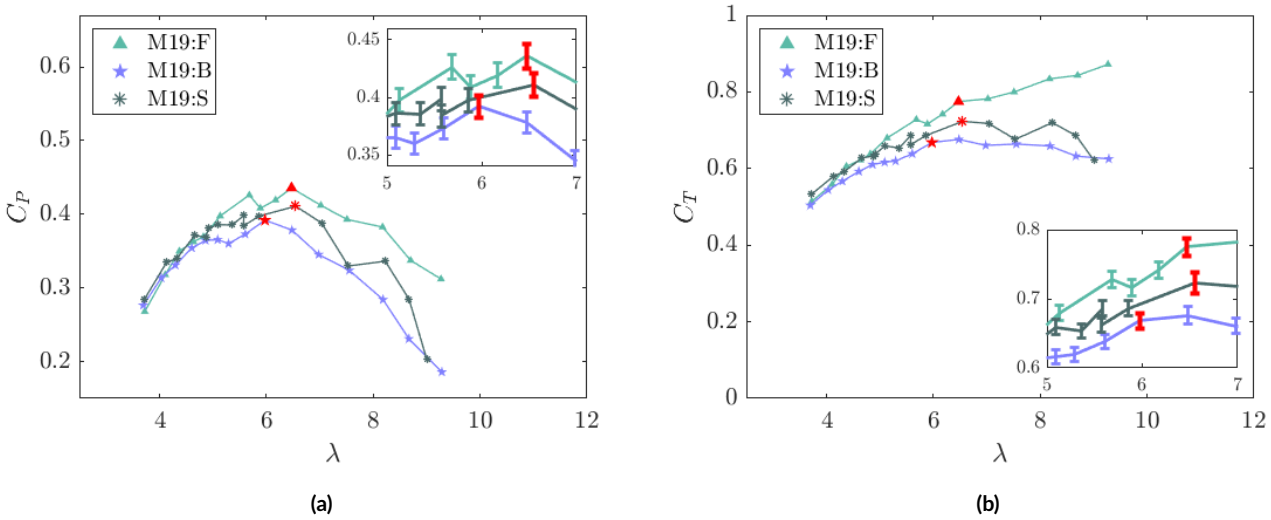

FIGURE 10 Effects of blade sweep for the wind turbine models with forward swept (F), backward swept (B) and straight (S) blades. **(a)** power coefficients and **(b)** thrust coefficients at different tip speed ratios, λ. The figure depicts the medium turbulence test case, M19, with $T_i = 18.82\%$ and $L_{ux}/D = 0.281$. The reference velocity was kept constant at $U_\infty = 12.5$ m/s for all the test cases. Thus, the tip speed ratio was only varying with the rotational velocity of the rotors, ω. The data points highlighted in red indicate the locations of the maximum power coefficients, $C_{P_{max}}$, for each test case. Error bars for C_P and C_T are shown in a zoomed view for the most interesting parts of the data.

The medium turbulence test case, M19, revealed more intriguing results. Figure 10 depicts the power and thrust coefficients for all the Ebaboard PW920 blades at $T_i = 18.82\%$ and $L_{ux}/D = 0.281$. Figure 10a shows that the forward swept blades (F) experienced a higher power coefficient for all tip speed ratios above $\lambda = 5$, compared to the straight blades (S). This increase in power output shows a corresponding increase in the thrust coefficient, as shown in Figure 10b. The maximum power coefficient was 6.0% higher for the forward swept blades and the thrust coefficient increased by 7.1% compared with the straight blades. The backward swept blades (B) had a slightly lower power output than the straight blades (S) throughout, but they also experienced a decrease in the thrust forces. Around the design tip speed ratio ($\lambda \approx 6$), the reduction in the power output was 4.6%, and the corresponding decrease in the thrust force was 7.6%. These results are summarized in Table 3. Results for the high turbulence test case, H23, are presented in Appendix D as they were very similar to what was presented here, for test case M19. It should be mentioned that measurements at low tip speed ratios ($\lambda < 4$) were not performed for the medium and high turbulence test cases because of safety considerations. All the wind turbine models experienced significant mechanical vibrations at high turbulence intensities and low tip speed ratios.

TABLE 3 Max power coefficients, $C_{P_{max}}$, for the test cases L03 and M19, with the corresponding tip speed ratios, λ, and thrust coefficients, C_T.

				Power coefficient			Thrust coefficient		
Test Case	**Blade Sweep**	$\mathbf{T_i}$ **[%]**	λ	$\mathbf{C_{P_{max}}}$	**Error**	$\mathbf{\Delta C_{P_{max}}}$ †	$\mathbf{C_T}$	**Error**	$\mathbf{\Delta C_T}$ ‡
L03:F	Forward swept	2.87	5.71	0.309	± 2.5 %	- 14.1 %	0.63	± 1.6 %	- 2.4 %
L03:B	Backward swept	2.87	4.43	0.307	± 2.7 %	- 14.7 %	0.55	± 1.6 %	- 14.6 %
L03:S	Straight	2.87	5.31	0.360	± 2.6 %		0.65	± 1.6 %	
M19:F	Forward swept	18.82	6.47	0.436	± 2.4 %	+ 6.0 %	0.77	± 1.7 %	+ 7.1 %
M19:B	Backward swept	18.82	5.97	0.392	± 2.5 %	- 4.6 %	0.67	± 1.6 %	- 7.6 %
M19:S	Straight	18.82	6.55	0.411	± 2.4 %		0.72	± 2.1 %	

†$\Delta C_{P_{max,F}} = \frac{C_{P_{max,F}} - C_{P_{max,S}}}{C_{P_{max,S}}}$, $\Delta C_{P_{max,B}} = \frac{C_{P_{max,B}} - C_{P_{max,S}}}{C_{P_{max,S}}}$.

‡$\Delta C_{T_F} = \frac{C_{T_F} - C_{T_S}}{C_{T_S}}$, $\Delta C_{T_B} = \frac{C_{T_B} - C_{T_S}}{C_{T_S}}$.

Figures 9 and 10 and Table 3 shows that the difference in solidity between the straight and swept models cannot account for the totality of the observed variations between the models. Particularly, the forward and backward swept blades had equal solidity, but show very different results. The main take-away from the presented results would be that the forward swept blades have a tendency to increase both the power and thrust coefficient, while for the backward swept blades they tend to decrease. This was particularly shown for the higher turbulence test cases, but individual differences were found for the low turbulence test case L03 as well. Here, the backward swept blades had a similar $C_{P_{max}}$ as the forward swept blades, but a significantly lower C_T.

The results agree well with literature, where the backward swept blades have shown the most promising results for passive load alleviation [14]. Test case M19:B in Table 3 shows how the thrust coefficient decreased more than the power coefficient. This indicates that it could be possible to increase the radius of the backward swept blades to obtain a similar power output as straight blades while the loads are slightly lower. This would be a positive effect for reducing the complexity of the structure and maintenance cost of wind turbines. In addition, this could indicate that an increased power output with similar loads is obtainable. Previous studies have suggested that this effect could be caused by a decrease in the angle of attack experienced by the airfoil sections throughout the blade span [14]. This study did not evaluate this claim any further, but additional results highlighting the stall region at low tip speed ratios are presented in Appendix D. For the forward swept blades, the results show that the potential increase in power output is accompanied by a higher increase in the thrust coefficient, which makes it more difficult to justify the use of this particular design. In that case, the radius of the straight blades could be increased instead to produce a higher power output and lower loads than for the forward swept blades.

3.3 | Effects of turbulence

The effects of varying the turbulent inflow conditions explained in Table 1 on the different model wind turbines introduced in Table 2 can be seen in Figures 11 and 12. This analysis focuses on two test cases, L03 and M19, with corresponding turbulence intensities of $T_i = 2.87\%$ and $T_i = 18.82\%$ and integral length scales of $L_{ux}/D = 0.049$ and $L_{ux}/D = 0.281$. In general, the model turbines experience an increased power output with an increase in the measured turbulent characteristics, as shown in Figure 11. However, the swept blades tend to have a higher relative increase than the straight blades. A quantifiable example of this is that the maximum power coefficient, $C_{P_{max}}$, of the forward swept blades (F), increase by 41% from test case L03 to M19, the backward swept blades (B) increase by 28%, while for the straight blades (S) the increase was only 14%. Another apparent effect experienced by all the wind turbine models is that the maximum power, $C_{P_{max}}$, was measured at a higher tip speed ratio, λ, for the test cases with higher turbulence intensities and integral length scales. This effect is consistent with previous observations, as reported by Gambuzza et al. [33]. It is however contradicting some of the previously presented results on the aluminum model [26,27,28]. In particular, Mikkelsen [28] reported that the power coefficient was found to decrease slightly with higher turbulence intensity. This contradiction could be accredited to the much lower turbulence intensities that were obtainable previously, without the use of an active grid. Bartl et al. [26] found a similar power coefficient at the design tip speed ratio for the homogeneous turbulence test case with a uniform grid and $T_i = 10\%$, compared with the reference case with a clean inlet. However, it was showed that the power increased marginally with higher turbulence for $\lambda > 6$. In the study performed by Li et

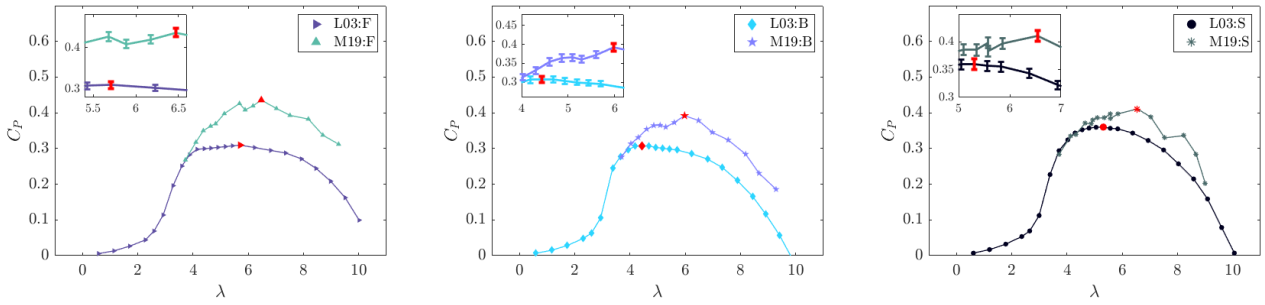

FIGURE 11 Effects of varying the turbulent inflow conditions on the power coefficients, C_P, of the wind turbine models at different tip speed ratios, λ. The reference velocity was kept constant at $U_\infty = 12.5$ m/s for all the test cases. Thus, the tip speed ratio was only varying with the rotational velocity of the rotors, ω. The figure depicts results for the low turbulence test case L03, where $T_i = 2.87\%$ and $L_{ux}/D = 0.049$, and the medium turbulence test case M19, where $T_i = 18.82\%$ and $L_{ux}/D = 0.281$. **(a)** forward swept blades (F), **(b)** backward swept blades (B), **(c)** straight blades (S). The data points highlighted in red indicate the locations of the maximum power coefficients, $C_{P_{max}}$, for each test case. Error bars for C_P are shown in a zoomed view for the most interesting parts of the data.

al.[48], it was found that the lift of the NREL S826 airfoil decreased marginally for the FST test cases with T_i between 1% and 2%, but increased substantially at $T_i > 2\%$. This could indicate that increasing the turbulence intensities further would also increase the experienced power output of the models. In addition, since Gambuzza et al.[33] found that the integral length scale strongly affects the power output, the differences cannot solely be explained by the turbulence intensities. Thus, the presented results seem to be in line with the literature considering the considerable increase in both turbulence intensities and integral length scales from test case L03 to M19.

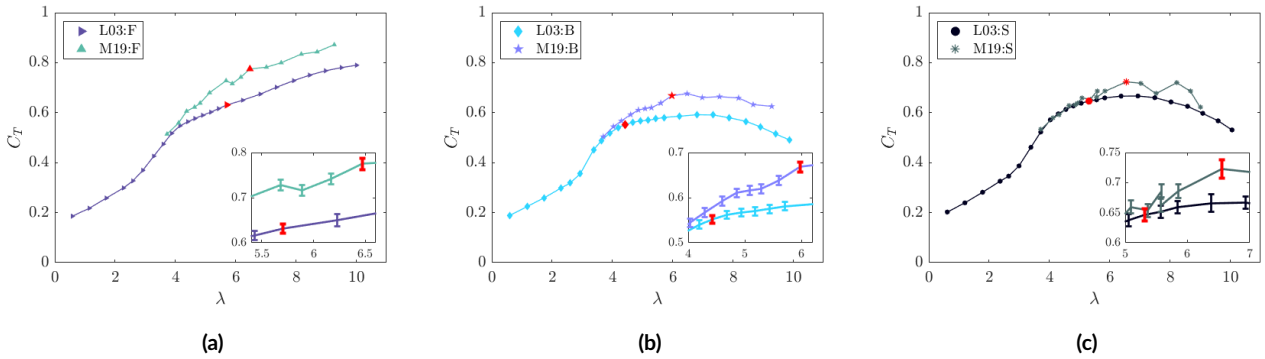

FIGURE 12 Effects of varying the turbulent inflow conditions on the thrust coefficients, C_T, of the wind turbine models at different tip speed ratios, λ. The reference velocity was kept constant at $U_\infty = 12.5$ m/s for all the test cases. Thus, the tip speed ratio was only varying with the rotational velocity of the rotors, ω. The figure depicts results for the low turbulence test case L03, where $T_i = 2.87\%$ and $L_{ux}/D = 0.049$, and the medium turbulence test case M19, where $T_i = 18.82\%$ and $L_{ux}/D = 0.281$. **(a)** forward swept blades (F), **(b)** backward swept blades (B), **(c)** straight blades (S). The data points highlighted in red indicate the locations of the maximum power coefficients, $C_{P_{max}}$, for each test case. Error bars for C_T are shown in a zoomed view for the most interesting parts of the data.

The thrust forces experienced by the models tend to increase with the inflow turbulence characteristics, but less so than the power. Figure 12 shows the effect of varying the turbulent inflow conditions on the thrust coefficients of all the wind turbine models. The thrust coefficient, C_T, at the same tip speed ratio as the previously reported differences in $C_{P_{max}}$ experienced an increase of 23% from test case L03 to M19 for the forward swept blades (F). The backward swept blades (B) underwent a 21% increase, while for the straight blades (S) it was 12%. The extracted data points detailed here are summarized in Table 3 and indicated as red dots in Figures 11 and 12. An unexpected discovery visualized in Figure 12b and 12c was that the thrust coefficients tend to decrease at high tip speed ratios, for both the backward swept (B) and straight (S) models, regardless of the inflow conditions. It is unclear what might have caused this behavior as the straight model depicted in Figure 12b should behave similarly to previous findings. For the aluminum model tested previously, the thrust coefficient was strictly increasing with the tip speed ratio[45]. This was found to be the case in the experiments that was performed by the author on the aluminum wind turbine model as well, as presented in Appendix A. It could be that this effect was caused by the choice of material, in that the straight Ebaboard PW920 model was found to behave substantially different from the aluminum wind turbine model during testing. Also worth noting with regards to the thrust measurements presented here is that the effective thrust on the rotor was not measured independently by the force balance. Therefore, the presented results include the total thrust acting on the wind turbine models as well as the experimental setup consisting of a tower shaft and nacelle. As drag is known to be dependent on the turbulent inflow conditions[55], this could have affected the presented results. However, the results for the aluminum model shown in Figure A2 in Appendix A shows that this effect was diminutive for those thrust measurements. As such, the discrepancies can possibly be associated with the differences in the material behavior instead.

Unfortunately, it was not possible to produce turbulence intensities between 3% and 18% for the current configuration. While the author recognizes that this imposed a limitation in the current study, the main purpose was to analyze the effects of blade sweep at the same turbulent inflow conditions. Thus, the somewhat limited discretization of turbulence intensities was considered sufficient herein. The relatively high jump in turbulence intensities from the low to medium FST test cases was a result of the distance from the active grid to the force balance that the experimental setup was mounted to in the wind tunnel. With this setup, the active grid was unable to produce lower turbulence intensities than 18% when operating, even with higher rotation frequencies, Ω. To counteract this effect, an option could be to increase the distance from the active grid to the wind turbine model. The decay of freestream turbulence with an increased streamwise distance from the active grid is a well-known phenomenon that could be utilized to produce lower turbulence intensities[56]. This would involve moving the force balance further downstream, and was therefore not considered practicable in this study.

4 | CONCLUSION

This study reported measurements of the aerodynamic performance of three horizontal axis wind turbine models with differing blade sweep orientations, namely forward swept blades, backward swept blades, and straight blades. The experiments used an active grid to provide different homogeneous, isotropic, freestream turbulence test cases with varying inflow conditions measured by the turbulence intensities, T_i, and integral length scales relative to the diameter of the rotors, L_{ux}/D. The analysis focused on two test cases in particular. L03, with $T_i = 2.87\%$ and $L_{ux}/D = 0.049$, and M19, with $T_i = 18.82\%$ and $L_{ux}/D = 0.281$.

Similar to previous studies, results show that the power coefficients of the wind turbine models increase with higher turbulence intensities. However, it was demonstrated that the various models were affected to different degrees. The forward swept blades experienced the most significant increase, where the maximum power coefficients were 41% higher for test case M19 than L03. The backward swept blades showed a 28% increase while it was only 14% for the straight blades. The thrust coefficients of the models were less affected by the turbulent inflow conditions. Nevertheless, the measured differences were still noticeable at 23%, 21%, and 12% for the forward swept, backward swept, and straight blades, respectively. Thus, turbulence increases the total drag on the system for all the models, although to different degrees.

By comparing the various wind turbine models at the same turbulent inflow conditions, it was found that at low turbulence intensities, the straight blades outperformed both the forward and backward swept blades. However, because of the significant increase in the performance of the swept blades at higher turbulence intensities, the results were different. For test case M19, the forward swept blades had a 6.0% higher maximum power coefficient than the straight blades. The corresponding increase in thrust coefficient at the same tip speed ratios was 7.1%. The backward swept blades had a 4.6% lower maximum power coefficient and decreased thrust coefficient of 7.6%. The CFD simulations performed by Kaya et al.[25] on similar wind turbine models support these findings. It is not yet clear what might be causing these effects on the aerodynamic performance of swept blades, but previous studies have indicated that it could be associated with changes in the angles of attack[14].

Future studies should include measurements with a greater discretization of the turbulence intensities, enabling more thorough analyses of the effects of turbulence on swept-bladed wind turbine models. To this end, attaining inflow conditions in line with what is experienced by utility-scale wind turbines in atmospheric boundary layers would be beneficial. In addition, wake measurements could be performed to investigate the complicated flow structures around the blades further. Other wind tunnel experiments that seek to explore the capabilities of wind turbine models with swept blades should carefully consider the manufacturing processes that are available to avoid Re-dependent results.

ACKNOWLEDGEMENTS

The author would like to thank the supervisors, Tania Bracchi and R. Jason Hearst, for creating an exciting project for the Master's thesis and for the opportunity to perform experiments in the newly refurbished wind tunnel at NTNU with a highly advanced active grid. In addition, the author sincerely thanks Halvor Haukvik for helping out with the production of the wind turbine blades, by operating the CNC machine. Lastly, the author gratefully acknowledges the help of Leon Li in performing hot-wire measurements and providing additional information about the active grid.

References

1. IEA . World Energy Outlook 2020 – Analysis. [Online] https://www.iea.org/reports/world-energy-outlook-2020; 2020. Accessed: 2021-06-16.

2. Manwell JF, McGowan JG, Rogers AL. *Wind energy explained: theory, design and application*. Wiley . 2011.

3. Herbert GJ, Iniyan S, Sreevalsan E, Rajapandian S. A review of wind energy technologies. *Renewable and sustainable energy Reviews* 2007; 11(6): 1117–1145.

4. IRENA . Future of wind. [Online] https://www.irena.org/publications/2019/Oct/Future-of-wind; 2019. Accessed: 2021-06-16.

5. Igwemezie V, Mehmanparast A, Kolios A. Current trend in offshore wind energy sector and material requirements for fatigue resistance improvement in large wind turbine support structures–A review. *Renewable and Sustainable Energy Reviews* 2019; 101: 181–196.

6. Veers PS, Ashwill TD, Sutherland HJ, et al. Trends in the design, manufacture and evaluation of wind turbine blades. *Wind Energy: An International Journal for Progress and Applications in Wind Power Conversion Technology* 2003; 6(3): 245–259.

7. Jackson K, Zuteck Mv, Van Dam C, Standish K, Berry D. Innovative design approaches for large wind turbine blades. *Wind Energy: An International Journal for Progress and Applications in Wind Power Conversion Technology* 2005; 8(2): 141–171.

8. Zuteck MD. *Adaptive blade concept assessment: curved planform induced twist investigation*. Sandia National Laboratories Clear Lake Shore, Texas, USA . 2002.

9. Ashwill TD, Veers PS, Locke J, Contreras I, Griffin D, Zuteck MD. Concepts for adaptive wind turbine blades. In: ASME 2002 Wind Energy Symposium. ; 2002: 56–69.

10. Ashwill T, Kanaby G, Jackson K, Zuteck M. Development of the sweep-twist adaptive rotor (STAR) blade. In: 8th AIAA Aerospace Sciences Meeting Including the New Horizons Forum and Aerospace Exposition. ; 2010: 1582.

11. Ashwill TD. Sweep-twist adaptive rotor blade: final project report.. tech. rep., Sandia National Laboratories; Albuquerque, New Mexico, USA: 2010.

12. Larwood SM, Zutek M. Swept wind turbine blade aeroelastic modeling for loads and dynamic behavior. In: WINDPOWER 2006. ; 2006; Pittsburgh, PA, USA.

13. Ding Y, Zhang X. An optimal design method of swept blades for HAWTs. *Journal of Renewable and Sustainable Energy* 2016; 8(4): 043303.

14. Pavese C, Kim T, Murcia JP. Design of a wind turbine swept blade through extensive load analysis. *Renewable energy* 2017; 102: 21–34.

15. Pavese C, Tibaldi C, Zahle F, Kim T. Aeroelastic multidisciplinary design optimization of a swept wind turbine blade. *Wind Energy* 2017; 20(12): 1941–1953.

16. Chen J, Shen X, Zhu X, Du Z. A Study on the Capability of Backward Swept Blades to Mitigate Loads of Wind Turbines in Shear Flow. *Journal of Energy Resources Technology* 2019; 141(8).

17. Sessarego M, Feng J, Ramos-García N, Horcas SG. Design optimization of a curved wind turbine blade using neural networks and an aero-elastic vortex method under turbulent inflow. *Renewable Energy* 2020; 146: 1524–1535.

18. Hansen MOL. *Aerodynamics of wind turbines*. Earthscan . 2007.

19. Verelst DR, Larsen TJ. Load Consequences when sweeping blades-a case study of a 5 MW pitch controlled wind turbine. tech. rep., Risø National Laboratory for Sustainable Energy, Technical University of Denmark (DTU); Roskilde, Denmark: 2010.

20. Larwood S, Dam CV, Schow D. Design studies of swept wind turbine blades. *Renewable Energy* 2014; 71: 563–571. doi: 10.1016/j.renene.2014.05.050

21. Larwood S, Dam CV. Dynamic analysis tool development for swept wind turbine blades. *Wind Energy* 2012; 16(6): 879–907. doi: 10.1002/we.1529

22. Barlas T, Pirrung GR, Ramos-García N, et al. Wind tunnel testing of a swept tip shape and comparison with multi-fidelity aerodynamic simulations. *Wind Energy Science Discussions* 2021; 2021: 1–20. doi: 10.5194/wes-2021-48

23. Amano R, Avdeev I, Malloy R, Shams MZ. Power, structural and noise performance tests on different wind turbine rotor blade designs. *International Journal of Sustainable Energy* 2013; 32(2): 78–95.

24. Khalafallah M, Ahmed A, Emam M. CFD study of some factors affecting performance of HAWT with swept blades. *International Journal of Sustainable Energy* 2017; 36(5): 489–501.

25. Kaya MN, Kose F, Ingham D, Ma L, Pourkashanian M. Aerodynamic performance of a horizontal axis wind turbine with forward and backward swept blades. *Journal of Wind Engineering and Industrial Aerodynamics* 2018; 176: 166–173. doi: 10.1016/j.jweia.2018.03.023

26. Bartl J, Mühle F, Schottler J, et al. Wind tunnel experiments on wind turbine wakes in yaw: effects of inflow turbulence and shear. *Wind Energy Science* 2018; 3(1): 329–343.

27. Bartl J, Sætran L. Blind test comparison of the performance and wake flow between two in-line wind turbines exposed to different turbulent inflow conditions. *Wind energy science* 2017; 2(1): 55–76.

28. Mikkelsen K. Effect of free stream turbulence on wind turbine performance. Master's thesis. Norwegian University of Science and Technology. Trondheim, Norway: 2013.

29. Hideharu M. Realization of a large-scale turbulence field in a small wind tunnel. *Fluid Dynamics Research* 1991; 8(1-4): 53.

30. Larssen JV, Devenport WJ. On the generation of large-scale homogeneous turbulence. *Experiments in fluids* 2011; 50(5): 1207–1223.

31. Hearst RJ, Lavoie P. The effect of active grid initial conditions on high Reynolds number turbulence. *Experiments in Fluids* 2015; 56(10): 1–20.

32. Mücke T, Kleinhans D, Peinke J. Atmospheric turbulence and its influence on the alternating loads on wind turbines. *Wind Energy* 2011; 14(2): 301–316.

33. Gambuzza S, Ganapathisubramani B. The effects of free-stream turbulence on the performance of a model wind turbine. *Journal of Renewable and Sustainable Energy* 2021; 13(2): 023304.

34. Li L, Hearst RJ, Ferreira MA, Ganapathisubramani B. The near-field of a lab-scale wind turbine in tailored turbulent shear flows. *Renewable Energy* 2020; 149: 735–748.

35. Rockel S, Peinke J, Hölling M, Cal RB. Dynamic wake development of a floating wind turbine in free pitch motion subjected to turbulent inflow generated with an active grid. *Renewable Energy* 2017; 112: 1–16.

36. Talavera M, Shu F. Experimental study of turbulence intensity influence on wind turbine performance and wake recovery in a low-speed wind tunnel. *Renewable Energy* 2017; 109: 363–371.

37. Jin Y, Liu H, Aggarwal R, Singh A, Chamorro LP. Effects of freestream turbulence in a model wind turbine wake. *Energies* 2016; 9(10): 830.

38. Bai CJ, Wang WC. Review of computational and experimental approaches to analysis of aerodynamic performance in horizontal-axis wind turbines (HAWTs). *Renewable and Sustainable Energy Reviews* 2016; 63: 506–519.

39. Bartl J, Mühle F, Sætran L. Wind tunnel study on power output and yaw moments for two yaw-controlled model wind turbines. *Wind Energy Science* 2018; 3(2): 489–502.

40. Krogstad PÅ, Eriksen PE. "Blind test" calculations of the performance and wake development for a model wind turbine. *Renewable energy* 2013; 50: 325–333.

41. Mühle F, Schottler J, Bartl J, et al. Blind test comparison on the wake behind a yawed wind turbine. *Wind Energy Science* 2018; 3(2): 883–903.

42. Krogstad PÅ, Sætran L, Adaramola MS. "Blind Test 3" calculations of the performance and wake development behind two in-line and offset model wind turbines. *Journal of Fluids and Structures* 2015; 52: 65–80.

43. Hearst RJ. The Use of Active Grids in Experimental Facilities. *Progress in Turbulence VIII* 2019: 173.

44. Krogstad PÅ, Lund J. An experimental and numerical study of the performance of a model turbine. *Wind Energy* 2012; 15(3): 443–457.

45. Krogstad PÅ, Adaramola MS. Performance and near wake measurements of a model horizontal axis wind turbine. *Wind Energy* 2012; 15(5): 743–756.

46. Adaramola M, Krogstad PÅ. Experimental investigation of wake effects on wind turbine performance. *Renewable Energy* 2011; 36(8): 2078–2086.

47. Somers DM. The S825 and S826 airfoils. tech. rep., National Renewable Energy Laboratory; Colorado, USA: 2005.

48. Li L, Hearst RJ. The influence of freestream turbulence on the temporal pressure distribution and lift of an airfoil. *Journal of Wind Engineering and Industrial Aerodynamics* 2021; 209: 104456.

49. Simis . Ashes - Wind turbine design with superpowers. [Online] https://www.simis.io/; . Accessed: 2021-06-16.

50. Burton T, Sharpe D, Jenkins N, Bossanyi E. *Wind energy handbook*. 2. Wiley Online Library . 2001.

51. Cantan JJCG. The effect of active grid-generated freestream turbulence on an aeroelastic NACA4412 airfoil. Master's thesis. Norwegian University of Science and Technology. Trondheim, Norway: 2021.

52. Chen T, Liou L. Blockage corrections in wind tunnel tests of small horizontal-axis wind turbines. *Experimental Thermal and Fluid Science* 2011; 35(3): 565–569.

53. Wheeler AJ, Ganji AR. *Introduction to engineering experimentation*. 199. Prentice Hall New Jersey . 1996.

54. Devinant P, Laverne T, Hureau J. Experimental study of wind-turbine airfoil aerodynamics in high turbulence. *Journal of Wind Engineering and Industrial Aerodynamics* 2002; 90(6): 689–707.

55. Pope SB. *Turbulent flows*. IOP Publishing . 2001.

56. Hearst RJ, Lavoie P. Decay of turbulence generated by a square-fractal-element grid. *Journal of Fluid Mechanics* 2014; 741: 567–584.

57. Wærness T. Design and Analysis of Swept Blades for a Horizontal Axis Wind Turbine. Engineering Fluid Mechanics, Specialization Project, NTNU; 2020.

APPENDIX

A ALUMINUM WIND TURBINE MODEL

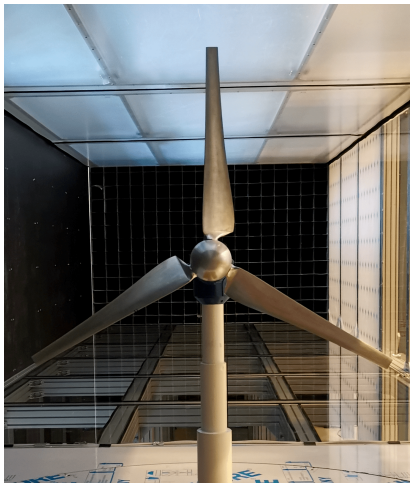

FIGURE A1 Front view of the aluminum wind turbine model. The rotational direction was anti-clockwise.

In addition to the aforementioned wind turbine models presented in this article, see Table 2, a somewhat separate study on a baseline model with straight, aluminum blades was performed as well. This was done to ensure that the performance measurements were correct, and to further analyze the influence of the highly turbulent inflow conditions. Here, it was possible to perform measurements for a full range of tip speed ratios and for a broader range of test cases (see Table A1) without safety limitations. This model was more robust and didn't experience any significant vibrations, as a result of the increased stiffness and stability of the aluminum blades. The aluminum model was not produced in this study and therefore the results are not included in the main part of this article. The results from these measurements are presented in Figure A2, where the aluminum model is denoted by A, to differentiate between the main results from the Ebaboard PW920 models presented previously.

It can be seen that the aluminum model also experienced an increase in the power coefficients for higher turbulence intensities, similarly to the Ebaboard PW920 models. The thrust coefficients were relatively constant for all the FST test cases, except for the high turbulence test cases H23 and H24 at high tip speed ratios, $\lambda > 8$.

TABLE A1 Overview of the inflow conditions for each test case that were used for the aluminum wind turbine model.

Test Case	Active grid	$\Omega \pm \omega'$ [Hz]	T_i [%]	L_{ux}/D	U_∞ [m/s]
REF	No		1.0		12.5
L03	Yes	0.0 ± 0.0	2.87	0.049	12.5
M18	Yes	7.0 ± 3.5	18.16	0.278	12.5
M19	Yes	5.0 ± 2.5	18.82	0.281	12.5
H23	Yes	1.0 ± 0.5	22.60	0.483	12.5
H24	Yes	0.5 ± 0.25	23.84	0.903	12.5

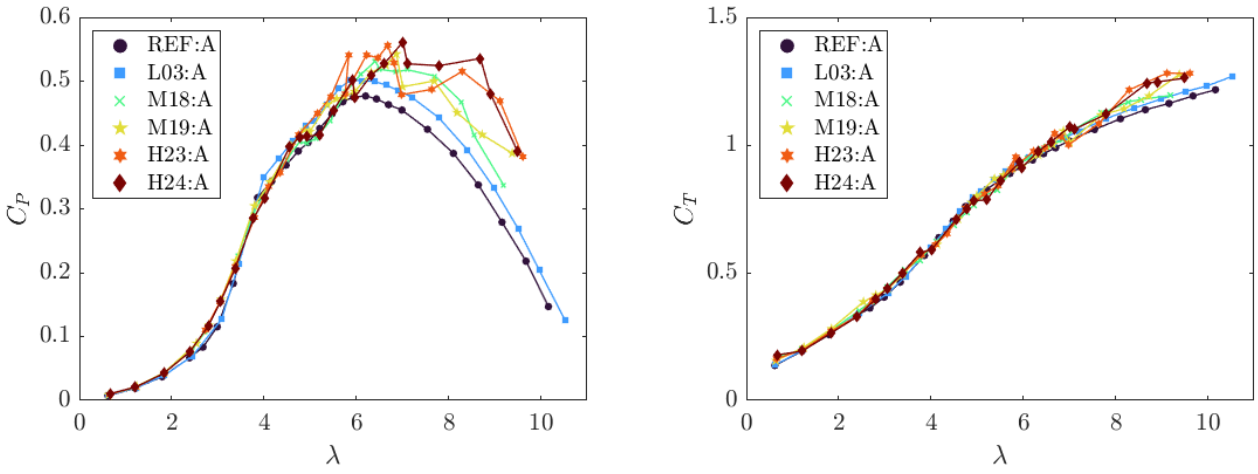

FIGURE A2 Effects of varying the turbulent inflow conditions on the power coefficients, C_P, and thrust coefficients, C_T of the wind turbine model with straight, aluminum blades (A) at different tip speed ratios, λ. The reference velocity was kept constant at $U_\infty = 12.5$ m/s for all the test cases. Thus, the tip speed ratio was only varying with the rotational velocity of the rotors, ω. The figure depicts results for all the FST test cases described in Table A1.

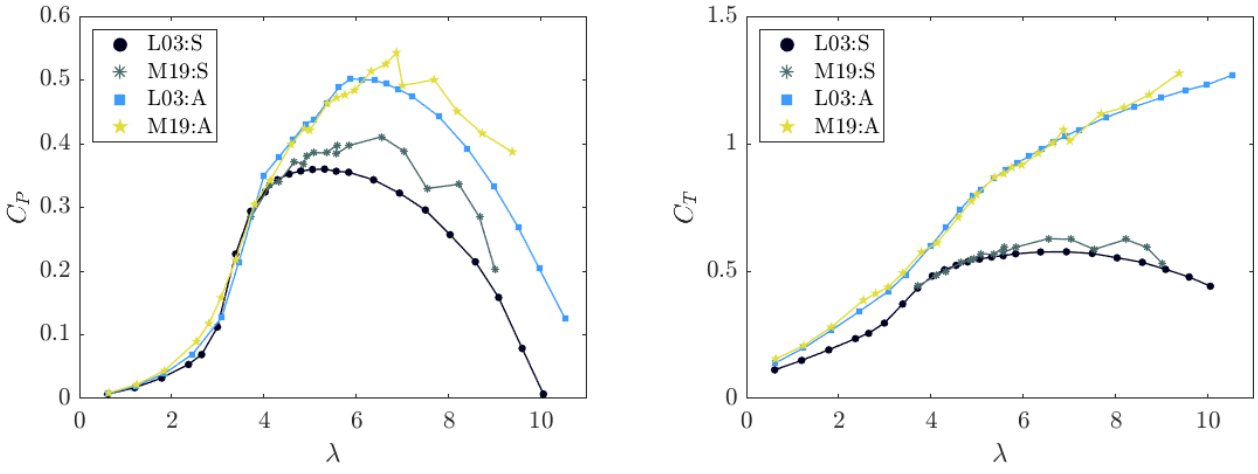

FIGURE A3 Effects of different material properties on the power coefficients, C_P, and thrust coefficients, C_T of the wind turbine models with straight blades at different tip speed ratios, λ. The reference velocity was kept constant at $U_\infty = 12.5$ m/s for all the test cases. Thus, the tip speed ratio was only varying with the rotational velocity of the rotors, ω. The figure depicts results for the low and medium turbulence test cases, L03 and M19, and for the straight wind turbine models produced in Ebaboard PW920 (S) and aluminum (A).

It should also be noted that there was a significant difference in the aerodynamic performance of the baseline models with straight, with different material and manufacturing complexities. As can be seen in Figure A3, the straight Ebaboard PW920 blades (S) have a significantly lower power output as well as lower experienced thrust, compared to the aluminum blades (A), at the same reference velocity and turbulent flow characteristics. This could be due to several factors, including lower chord lengths because of a higher tolerance at the trailing edges, mechanical vibrations caused by lower stiffness and stability, and human errors in the manufacturing process where sandpaper was used. For this study, it was therefore necessary to produce all the blades in the same material as it would not be possible to compare the models that were produced in different materials directly. This severely increased the time spent on manufacturing, but was necessary to produce comparable results.

B PRELIMINARY ASHES STUDY

A preliminary study was conducted by the author, as a basis for the production of the swept blades considered in this article. This section serves as a summary of the results that were found in that study, as presented in a separate report[57]. The aerodynamic performances of swept wind turbine blades were investigated, by use of the simulation software ASHES[49], which implements the well-established Blade Element Momentum (BEM) method. The radius of the blades were kept constant to be able to isolate the impacts of the different swept designs on the aerodynamic performances of the blades. The effect of the location of the sweep startup and tip offset of the swept blades was assessed. In particular, the power coefficients, C_P, and thrust coefficients, C_T, were analyzed at design tip speed ratio for the different blade designs. The swept blades were compared with a baseline wind turbine model with straight blades and a diameter of 0.9 m that has been tested extensively in previous studies, both numerically and experimentally. A 4-digit code was developed to differentiate between the swept blades. The first 2 digits express the relative sweep startup, r_{ss}/R, and the last 2 digits express the relative tip offset, d_s/R. Figure B4 shows the evaluated models with the most promising results.

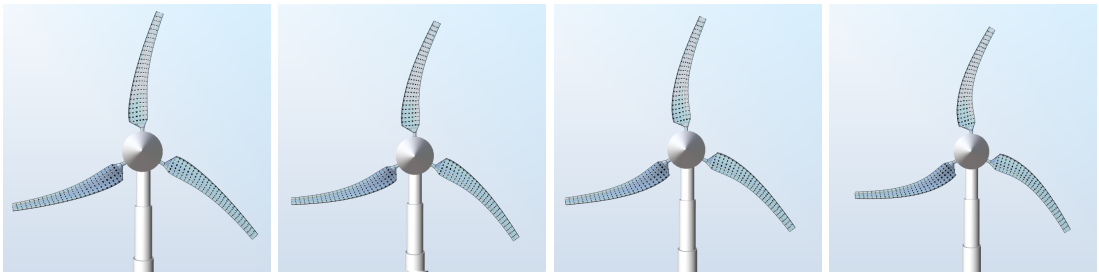

(a) 3515 **(b)** 3520 **(c)** 5515 **(d)** 5520

FIGURE B4 The wind turbine models implemented in ASHES with forward swept blades.

The swept blades with relative sweep startup, $P_{rss} = 0.55$, and relative tip offset, $P_{ds}/R = 0.20$, was found to give the most significant increase in the power output of the wind turbine. Specifically, the increase in C_P was 3.21% compared to the baseline model with straight blades at the design tip speed ratio ($\lambda = 6$). For this particular blade design, it was found that the corresponding increase in C_T was 4.77% and the increase in blade length because of the curvature of the blades was 2.76%. In conclusion, it was found that introducing sweep in the blades could potentially increase the power output of the wind turbine, but also increase the thrust coefficient and thus the loads experienced by the structure. Also, it was found that the BEM method in ASHES was not able to capture the difference in sweep direction, namely forward and backward swept blades, as the results were identical for both sweep directions. This could be accredited to the simplifying assumptions in the BEM method, in particular as it neglects some of the potentially present 3D effects.

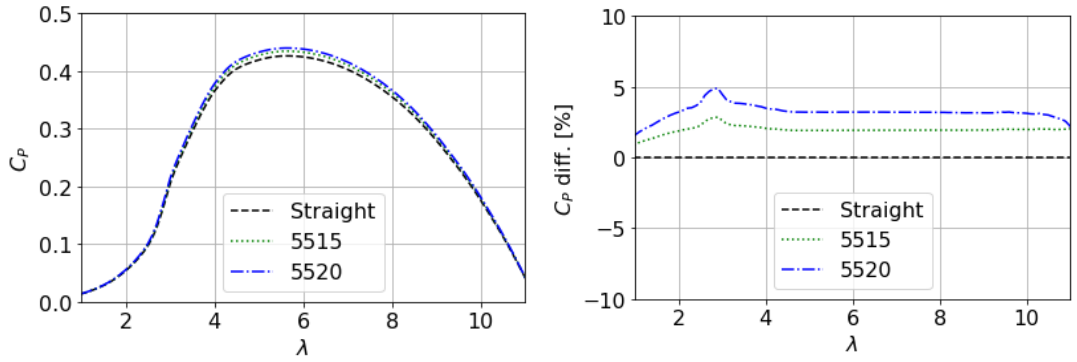

(a) Power coefficients vs. tip speed ratio. **(b)** Percentage differences in C_P.

FIGURE B5 Power coefficients compared to the baseline model for the wind turbine models with $r_{ss}/R = 0.55$ and $d_s/R = 0.15$ and 0.20.

As can be seen in Figure B6 and Figure B5, the results from ASHES for these models showed a relative increase in the power coefficients for all tip speed ratios. The only exception was for the C_P values of 3515 and 3520 for $\lambda > 10$, as shown in Figure B6b. The percentage difference in C_P were found to be relatively similar for a broad range of tip speed ratios. Some particularly interesting results were found for $\lambda \approx 3$, where the swept blades seemed to experience a slightly higher increase in the power output in the stall region.

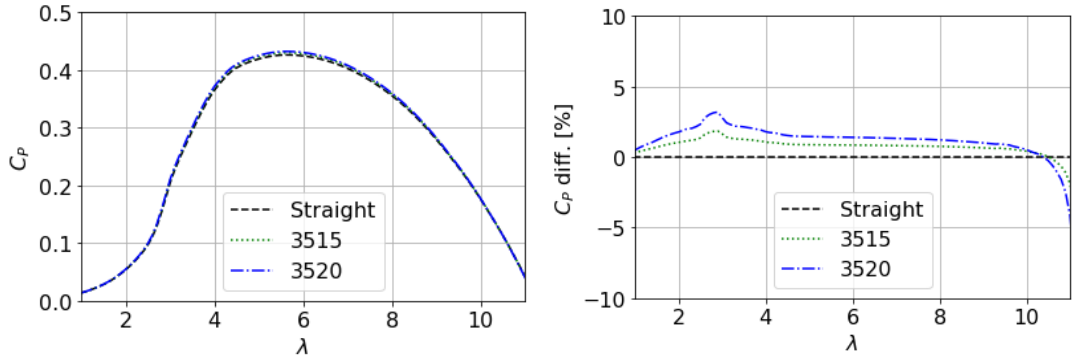

(a) Power coefficients for different TSR.

(b) Percentage differences in C_P.

FIGURE B6 Power coefficients compared to the baseline model for the wind turbine models with $r_{ss}/R = 0.35$ and $d_s/R = 0.15$ and 0.20.

As mentioned previously, it was decided to produce both the forward and backward swept blades with relative sweep startup, $r_{ss}/R = 0.35$, and relative tip offset, $d_s/R = 0.20$. The wind turbine model depicted in Figure B4d with $r_{ss}/R = 0.55$ and $d_s/R = 0.20$ was thought to introduce added manufacturing complexities.

C UNCERTAINTY ANALYSIS

The procedure for calculating the uncertainties in this experimental study is based on the simplified fractional uncertainty, as explained by Wheeler et al.[53], p. 201. For each value, R, the total uncertainty, W_R, has been calculated based on the total uncertainties of each contributing factor $x_1, ..., x_n$ in R. Here, $R = C_P, C_T, \lambda$ (see Equations (1) to (3)).

$$R = x_1^a x_2^b ... x_n^N, \tag{C1}$$

$$\frac{W_R}{R} = \left((a\frac{W_1}{x_1})^2 + (b\frac{W_2}{x_2})^2 + ... + (N\frac{W_n}{x_n})^2 \right)^{1/2}, \tag{C2}$$

The total uncertainty of the measured mean value of x, $W_{\overline{x}}$, is a combination of the random uncertainty, $P_{\overline{x}}$, and the systematic uncertainty, B_x, in the measurements.

$$W_{\overline{x}} = \left((B_x)^2 + (P_{\overline{x}})^2 \right)^{1/2}, \tag{C3}$$

$$P_{\overline{x}} = \frac{tS_{\overline{x}}}{\sqrt{n}}, \tag{C4}$$

where $S_{\overline{x}}$ is the standard deviation of the mean, n is the number of measurements that the mean value is obtained from, and t is the value from a student t-distribution. For a large number of samples, as in this study, $t = 1.960$.

D ADDITIONAL RESULTS

This section includes the remaining results from the main study that were not presented in Section 3. Of the FST test cases detailed in Table 1, the results from REF and H23 are presented here. The reference test case, REF, for all the wind turbine models without the active grid is shown in Figure D7. Figure D8 shows similar results for the high turbulence test case H23 as presented in Figure 10 for test case M19. Table D2 summarizes the main findings from these test cases, similarly to what was presented in Table 3. As mentioned previosuly in Section 3.1, the results from the reference test case showed Re-dependent behavior, similar to what has been presented in previous studies for the aluminum model at lower wind speeds[44,45] ($U_\infty < 9$ m/s). This is especially prevalent in Figure D7a for the forward (F) and backward (B) swept blades, around the design tip speed ratio ($\lambda \approx 6$).

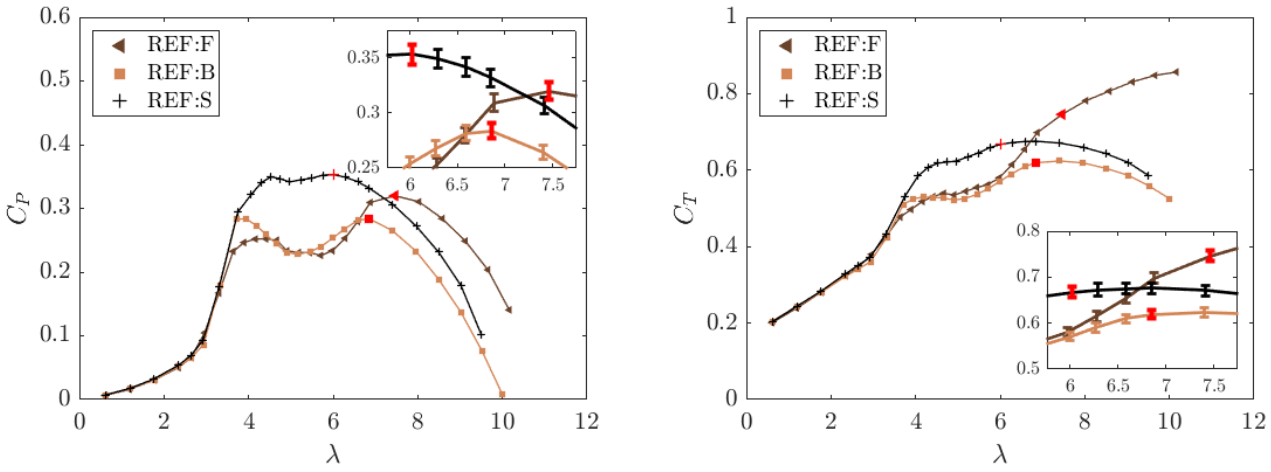

FIGURE D7 Effects of blade sweep for the wind turbine models with forward swept (F), backward swept (B) and straight (S) blades. **(a)** power coefficients and **(b)** thrust coefficients at different tip speed ratios, λ. The figure depicts the reference test case, REF, with $T_i = 1\%$. The reference velocity was kept constant at $U_\infty = 12.5$ m/s for all the test cases. Thus, the tip speed ratio was only varying with the rotational velocity of the rotors, ω. The data points highlighted in red indicate the locations of the maximum power coefficients, $C_{P_{max}}$, for each test case. Error bars for C_P and C_T are shown in a zoomed view for the most interesting parts of the data.

TABLE D2 Max power coefficients, $C_{P_{max}}$, for the test cases REF and H23, with the corresponding tip speed ratios, λ, and thrust coefficients, C_T.

				Power coefficient			Thrust coefficient		
Test Case	**Blade Sweep**	$\mathbf{T_i}$ **[%]**	λ	$\mathbf{C_{P_{max}}}$	**Error**	$\mathbf{\Delta C_{P_{max}}}$ †	$\mathbf{C_T}$	**Error**	$\mathbf{\Delta C_T}$ ‡
REF:F	Forward swept	1.0	7.46	0.320	± 2.4 %	- 9.4 %	0.75	± 1.6 %	+ 11.7 %
REF:B	Backward swept	1.0	6.86	0.284	± 2.4 %	- 19.6 %	0.62	± 1.6 %	- 7.2 %
REF:S	Straight	1.0	6.03	0.353	± 2.5 %		0.67	± 1.6 %	
H23:F	Forward swept	22.60	6.36	0.440	± 2.5 %	+ 3.0 %	0.76	± 1.6 %	+ 4.4 %
H23:B	Backward swept	22.60	5.77	0.392	± 2.5 %	- 8.1 %	0.65	± 1.6 %	- 11.6 %
H23:S	Straight	22.60	6.64	0.427	± 2.5 %		0.73	± 2.0 %	

†$\Delta C_{P_{max,F}} = \frac{C_{P_{max,F}} - C_{P_{max,S}}}{C_{P_{max,S}}}$, $\Delta C_{P_{max,B}} = \frac{C_{P_{max,B}} - C_{P_{max,S}}}{C_{P_{max,S}}}$.

‡$\Delta C_{T_F} = \frac{C_{T_F} - C_{T_S}}{C_{T_S}}$, $\Delta C_{T_B} = \frac{C_{T_B} - C_{T_S}}{C_{T_S}}$.

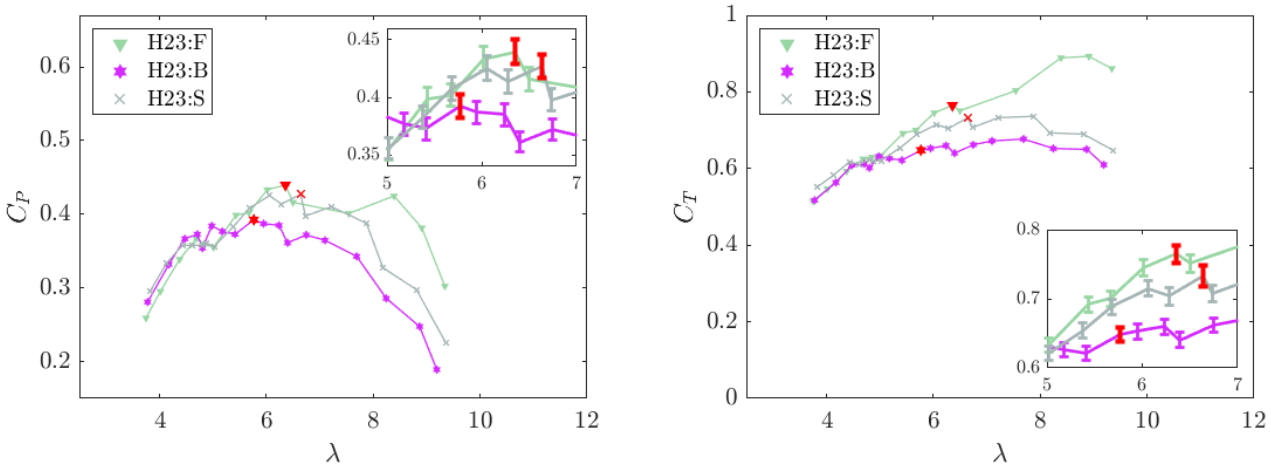

FIGURE D8 Effects of blade sweep for the wind turbine models with forward swept (F), backward swept (B) and straight (S) blades. **(a)** power coefficients and **(b)** thrust coefficients at different tip speed ratios, λ. The figure depicts the high turbulence test case, H23, with $T_i = 22.60\%$ and $L_{ux}/D = 0.483$. The reference velocity was kept constant at $U_\infty = 12.5$ m/s for all the test cases. Thus, the tip speed ratio was only varying with the rotational velocity of the rotors, ω. The data points highlighted in red indicate the locations of the maximum power coefficients, $C_{P_{max}}$, for each test case. Error bars for C_P and C_T are shown in a zoomed view for the most interesting parts of the data.

In addition to the remaining results from the REF and H23 test cases, some additional results on the torque coefficient, C_Q, which is given by

$$C_Q = \frac{Q}{\frac{1}{2}\rho U_\infty^2 AR} = \frac{C_P}{\lambda}, \tag{D5}$$

might help in estimating the location of maximum torque experienced by a model wind turbine during operation. Furthermore, the rotor speed power coefficient, K_P, which is given by

$$K_P = \frac{P}{\frac{1}{2}\rho(\omega R)^3 A} = \frac{C_P}{\lambda^3}. \tag{D6}$$

can be presented with the advance ratio, $J = 1/\lambda$, to produce a K_P-J curve [50]. A principal feature of utilizing the somewhat unfamiliar rotor speed power coefficient and advance ratio curve is determining when stall arises [45]. These coefficients were not included in the main analysis as they are calculated from the same torque measurements that were used for C_P, and thus contain no additional information. However, they are included here as they do highlight the behaviour of the wind turbine models at low tip speed ratios ($\lambda < 5$). Consequently, they are only presented for test cases REF and L03 as measurements for $\lambda < 4$ were not performed for the high turbulence test cases. From Figure D9a it becomes clear that the backward swept blades (B) experience a slightly higher maximum torque than the forward swept blades (F). Figure D9b shows that the drop in K_P is quite abrupt for all the models at $J \approx 0.3$ ($\lambda \approx 3.3$). Then the rotor speed power coefficient increases gradually again for higher advance ratios. As can be seen in the figure, the backward swept blades experience a sharper peak than the straight blades, and the forward swept blades experience a more rounded peak. This indicates that the rotor blades stall more abruptly for the backward swept blades and that the forward swept blades stall more gradually. This in turn could be associated with a potential decreased angle of attack for the backward swept blades, and an increased angle of attack for the forward swept blades.

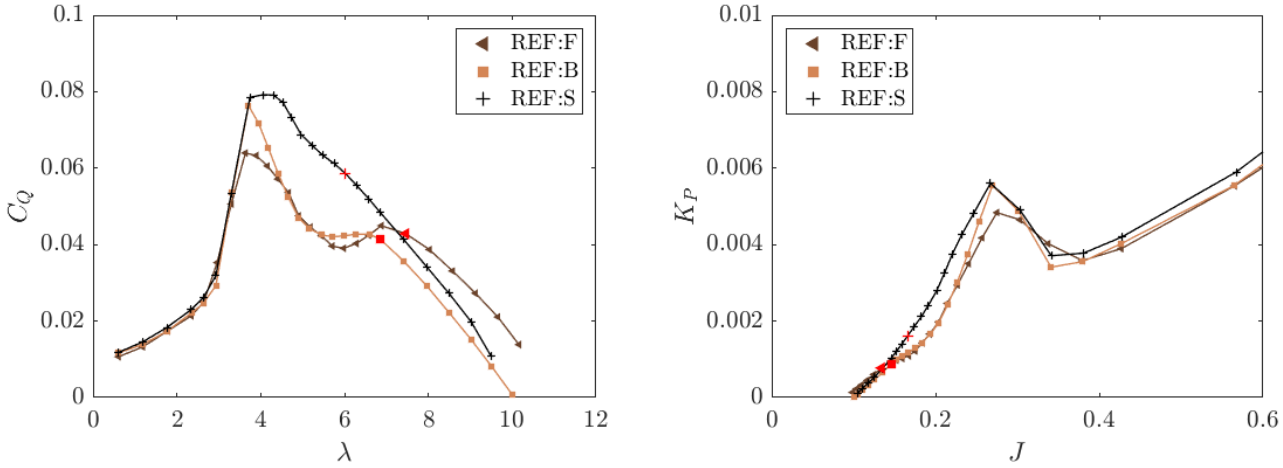

(a) **(b)**

FIGURE D9 Effects of blade sweep for the wind turbine models with forward swept (F), backward swept (B) and straight (S) blades. **(a)** torque coefficients, **(b)** rotor speed power coefficients at different tip speed ratios, λ, and advance ratios, $J = 1/\lambda$. The figure depicts the reference test case, REF, with $T_i = 1\%$. The reference velocity was kept constant at $U_\infty = 12.5$ m/s for all the test cases. Thus, the tip speed ratio was only varying with the rotational velocity of the rotors, ω. The data points highlighted in red indicate the locations of the maximum power coefficients, $C_{P_{max}}$, for each test case.

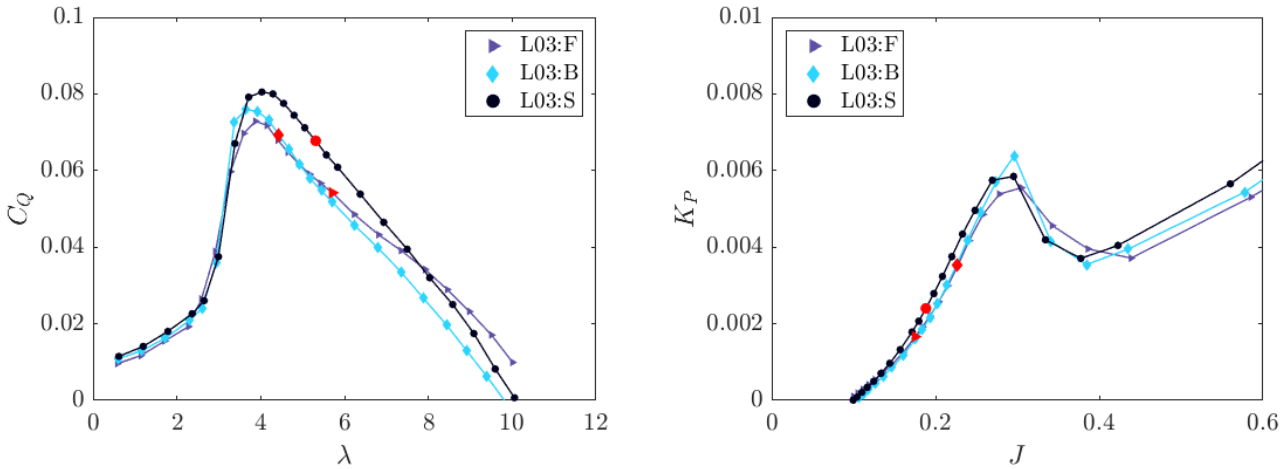

(a) **(b)**

FIGURE D10 Effects of blade sweep for the wind turbine models with forward swept (F), backward swept (B) and straight (S) blades. **(a)** torque coefficients, **(b)** rotor speed power coefficients at different tip speed ratios, λ, and advance ratios, $J = 1/\lambda$. The figure depicts the low turbulence test case, L03, with $T_i = 2.87\%$ and $L_{ux}/D = 0.049$. The reference velocity was kept constant at $U_\infty = 12.5$ m/s for all the test cases. Thus, the tip speed ratio was only varying with the rotational velocity of the rotors, ω. The data points highlighted in red indicate the locations of the maximum power coefficients, $C_{P_{max}}$, for each test case.

NTNU

Norwegian University of
Science and Technology